Region II Storm Surge Project - Development of Wind and Pressure Forcing in Tropical and Extratropical Storms

September 2014

FEMA

Federal Emergency Management Agency
Department of Homeland Security
500 C Street, SW
Washington DC, 20472

Contract: HSFEHQ-09-D-0369
Task Order: HSFE02-09-J-0001

This document was prepared by

RAMPP
8401 Arlington Blvd.
Fairfax, VA 22031

TABLE OF CONTENTS

Figures

Tables

Appendices

ADCIRC	ADvanced CIRCulation Model for Oceanic, Coastal and Estuarine Waters
C	Celsius
CISL	Computational and Information Systems Laboratory
C-MAN	Coastal-Marine Automated Network
CMAS	Circular Map Accuracy Standards
deg	degree
ESA	European Space Agency
ESDU	Engineering Sciences Data Unit
FEMA	Federal Emergency Management Agency
FGDC	Federal Geographic Data Committee
g	gram
GMT	Greenwich Mean Time
GPS	Global Positioning System
HRD	Hurricane Research Division
ICOADS	International Comprehensive Ocean Atmosphere Data Set
ISH	Integrated Surface Hourly
JPL	Jet Propulsion Laboratory
JPM	Joint Probability Method
kg	kilogram
kts	knots
m	meter
mb	millibar
met	meteorological
MORPHOS	Modeling of Relevant Physics of Sedimentation
m/s	meters per second
NASA	National Aeronautics and Space Administration
NCAR	National Center for Atmospheric Research
NCEP	National Centers for Environmental Prediction
NDBC	National Data Buoy Center
NHC	National Hurricane Center
NHC/TPC	National Hurricane Center/Tropical Prediction Center
Nmi	Nautical Mile
NOAA	National Oceanic and Atmospheric Administration
NOS	National Ocean Service
NRA	NCEP/NCAR 40-Year Reanalysis Project

NSF	National Science Foundation
NWS	National Weather Service
ODGP	Ocean Data Gathering Program
OWI	Oceanweather Incorporated
PBL	Planetary Boundary Layer
RAMPP	Risk Assessment, Mapping, and Planning Partners
RDA	Research Data Archive
RMW	Radius of Maximum Winds
UnSWAN	Unstructured Grids In Simulating WAves Nearshore
TAWS	Tropical Analyst Workstation
USEC	U.S. East Coast
UTC	Coordinated Universal Time

SECTION ONE INTRODUCTION

In 2009, the Federal Emergency Management Agency (FEMA) authorized the Risk Assessment, Mapping, and Planning Partners (RAMPP) Joint Venture to initiate a study of coastal flooding risk in the area of the New Jersey coast from Cape May to the New Jersey–New York border at the Hudson River. This area included New York City as defined by its borders on Long Island, the mainland and the bounding waterways. Oceanweather Inc. (OWI) is participating in the following elements of project: (1) assembly of comprehensive historical meteorological data and reanalysis of the track, intensity and internal structure of the wind and pressure fields of a population of historical high-ranked U.S. East Coast (USEC) hurricanes to provide characteristic storm parameters needed for the development of probability distributions from which synthetic storms will be specified; (2) storm selection and delivery to RAMPP of wind and pressure fields of maximum achievable accuracy in small populations of actual high-ranked historical storms to calibrate/validate the ADvanced CIRCulation Model (ADCIRC) hydrodynamic model; (3) development of wind and pressure fields for the full target population of historical extratropical storms; (4) wind and pressure field generation to populate Joint Probability Method (JPM) tropical systems to be hindcast; and finally, general consultations throughout the project.

SECTION TWO TROPICAL CYCLONE PARAMETER ANALYSIS AND SYNOPTIC CLIMATOLOGY

2.1 APPROACH

The development of the tropical cyclone parameter synoptic climatology consists of two major subtasks: (1) data assembly from previous relevant studies of USEC hurricanes at OWI, from updates and reanalysis of previous storm track and intensity databases maintained by the U.S. government, and, especially for older storms, rescue and digitization of data from fragile microfilm and paper data media; (2) application of a new tropical analyst workstation (TAWS) to define the characteristics of tropical cyclones in the region with a minimal number of parameters consistent with present state of knowledge about the structure of these storms; the input data requirements of OWI's numerical cyclone planetary boundary layer model is also consistently applied to the reanalysis and specification of wind fields in actual historical and synthetic USEC hurricanes.

The population of storms addressed consists of 30 major hurricanes since 1938. OWI's recently introduced TAWS is applied to the reanalysis of the temporal evolution of each cyclone over the period of storm history, beginning when the storm could be expected to generate sea and coastal surge that affects the study area. TAWS allows for the description of the radial pressure distribution in the boundary layer using a single or a double exponential analytical formulation and allows the analyst to iterate the Planetary Boundary Layer (PBL) model against available surface wind measurements. The full potential of TAWS is realized during aircraft reconnaissance and research at flight level and through remotely sensed surface meteorological measurements of wind and pressure in a cyclone. OWI studies of storms in basins with no aircraft data, such as pre-1986 North Pacific typhoons and cyclones in other basins, have also shown that even when storms move through sparse arrays of marine observation and surface wind and pressure measurements from coastal and island weather stations, TAWS can often be applied effectively. This was also the case for the earlier USEC hurricanes selected for reanalysis in this study.

The double exponential model provides twice the number of storm parameters than have been used in recent similar FEMA-sponsored coastal risk assessment studies for the Gulf of Mexico and southeast Atlantic coast. The added complexity is necessary because even in those areas many well-documented hurricanes exhibit a more complicated structure. Hurricanes that affect the study area, especially later in the season, tend to rapidly acquire a non-tropical structure with a consequent departure of the radial wind and pressure profile from the simple structure of tropical cyclones in tropical latitudes.

For the purposes of developing probability distributions from which synthetic storms will be generated, it may be necessary to reduce the number of parameters insofar as possible. Details can be found in the Joint Probability Analysis Of Hurricane and Extratropical Flood Hazards report (RAMPP, 2014). This report also includes some assessment of whether there is any tendency toward internal parameter correlations that might allow simplification of the number of parameters, resulting statistical distributions, and reduction of the number of synthetic storms.

2.2 DATA SOURCES

2.2.1 In situ Data

The *in situ* dataset included buoys, ship reports, coastal-manned measurement platforms and land-based observations from a variety of sources. U.S. buoy and Coastal-Marine Automated Network (C-MAN) data came from the National Oceanic and Atmospheric Administration (NOAA) Marine Environmental Buoy Database on CD-ROM. Ship data came from the International Comprehensive Ocean Atmosphere Dataset (ICOADS) described by Worley et al. (2005). Most land-based observations came from the Integrated Surface Hourly (ISH) dataset obtained from the National Climatic Data Center. Coastal winds and water level measurements were obtained from the National Ocean Service archives. Additional coastal and overwater measurements primarily from university measurement programs were provided by the collection agency or archived from real-time data posted on the National Data Buoy Center website. Additional data, including time series and storm maxima conditions, were obtained from miscellaneous storm reports, Monthly Weather Review summaries, newspaper articles, and National Hurricane Center (NHC) storm wallets.

All wind speeds were adjusted to 10-minute neutral winds following the approach described in Cardone et al. (1990), which adjusts winds for both height and stability using a logarithmic wind profile. Where continuous 10-minute winds were available, a 30-minute average wind was obtained via equal weight averaging.

2.2.2 Satellite Derived Wind Measurements

TOPEX and JASON-1 data were obtained from the National Aeronautics and Space Administration (NASA) Physical Oceanography Distributed Active Archive Center at the Jet Propulsion Laboratory/California Institute of Technology (JPL). ENVISAT data were provided by the European Space Agency (ESA). All datasets were decoded using the recommended quality controls described in each respective document.

Scatterometer winds were obtained from the ERS-1, ERS-2, NSCAT and QUIKSCAT instruments. ERS data were obtained from the French Research Institute for Exploration of the Sea (Ifremer), while NSCAT and QUIKSCAT data were obtained from JPL. All datasets were decoded using the recommended quality controls described in each respective document.

2.2.3 Wind and Pressure Fields

National Center for Environmental Prediction/National Center for Atmospheric Research (NCAR) 40-Year Reanalysis Project (NRA) (Kalnay et al., 1996) sea-level pressure fields were applied in specification of the far-field pressures for tropical systems from 1948 through the present using a technique described in Knaff and Zher (2007) which estimates the far field from an annulus of atmospheric pressures surrounding each storm. Determination of far-field pressures for tropical systems before 1948 applied an archive of daily northern hemisphere surface pressures from the Research Data Archive (RDA) which is maintained by the Computational and Information Systems Laboratory (CISL) at the NCAR. NCAR is sponsored by the National Science Foundation (NSF). The original data are available from the RDA (http://dss.ucar.edu) in dataset number ds010.0.

2.2.4 Flight Level Aircraft Data

Aircraft reconnaissance in the Atlantic basin started in the 1940s with Air Force and Navy missions into storms and continues today with planes from both NOAA and the 53rd Weather Reconnaissance Squadron of the Air Force. Early reconnaissance data was typically archived in microfilm form, which needed to be tediously scanned and the data manually extracted and typed for use in tropical analysis. Figure 1 shows a microfilm copy of data obtained during Hurricane Donna in 1960. Storms from the late 1970s onward are available in electronic form primarily from either the NHC Tropical Prediction Center (NHC/TPC) or the Hurricane Research Division (HRD). Data availability and data formats vary in the archive, even within the same storm year. NOAA and Air Force data are generally in different formats and not consistently available from the same archive source. Thus, the assembly and processing of reconnaissance data to a common format for tropical analysis required extensive manual work and quality control. All flight-level data are processed to the common format shown in Table 1; not all datasets contain all the variables detailed.

Table 1. Tropical reconnaissance common data format

Variable	Description
Date/Time	Observation Time (GMT)
Lat	Latitude (deg)
Long	Longitude (deg)
StdPres	Standard Pressure (mb)
Zp	Height (m) of Standard Pressure Surface
Ws	Flight Level Wind Speed (m/s)
Wd	Flight Level Wind Direction (met deg)
Temp	Flight Level Temperature (C)
DewPt	Flight Level Dewpoint (C)
H2O	Liquid Water Content (g/kg)
RadarAlt	Height (m) indicated by radar
PresAlt	Height (m) indicated by pressure
Source	Data Source
StormLat	Latitude (deg)
StormLong	Longitude (deg)
Bearing	deg from storm
StmBear	Bearing relative to storm (45=Right Front Quadrant)
Range	km from storm
RadWind	Flight Level Radial component of wind (m/s)
TanWind	Flight Level Tangential component of wind (m/s)
VertWind	Flight Level Vertical component of wind (m/s)
SLP	Sea Level Pressure (mb)
SLPMeth	How SLP was obtained (measured/estimated)
SFCWs	Surface Wind Speed (m/s) 30-Min Average @ 10 m
SFCWsMeth	How SFCWs was obtained (measured/estimated)

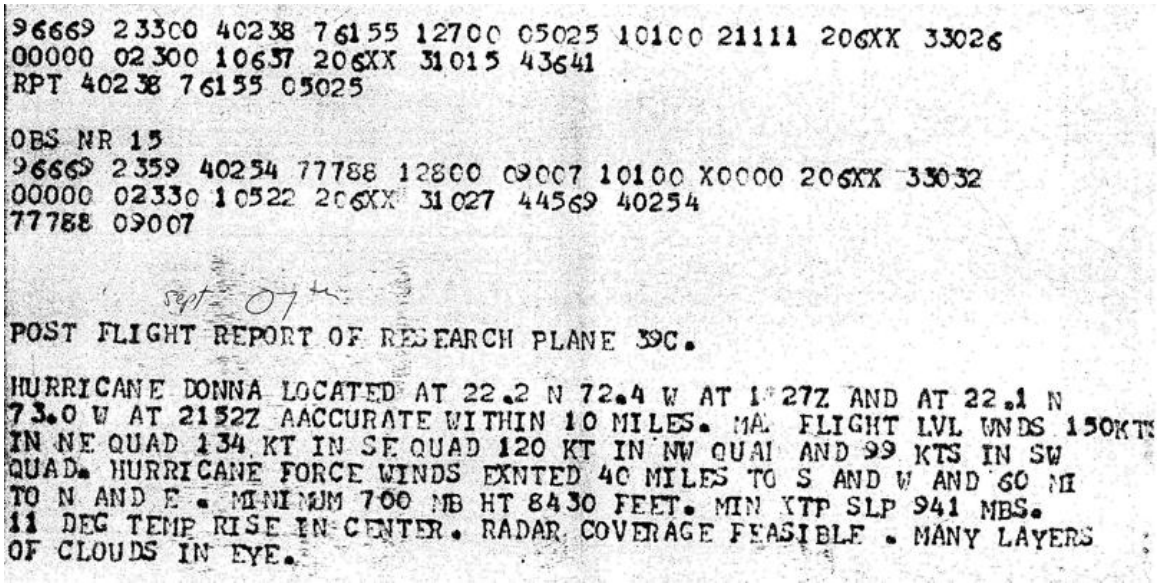

96669 23300 40238 76155 12700 05025 10100 21111 206XX 33026
00000 02300 10657 206XX 31015 43641
RPT 40238 76155 05025

OBS NR 15
96669 2359 40254 77788 12800 09007 10100 X0000 206XX 33032
00000 02330 10522 206XX 31027 44569 40254
77788 09007

sept 07

POST FLIGHT REPORT OF RESEARCH PLANE 39C.

HURRICANE DONNA LOCATED AT 22.2 N 72.4 W AT 1[illegible]27Z AND AT 22.1 N
73.0 W AT 2152Z AACCURATE WITHIN 10 MILES. MAX FLIGHT LVL WNDS 150KTS
IN NE QUAD 134 KT IN SE QUAD 120 KT IN NW QUAD AND 99 KTS IN SW
QUAD. HURRICANE FORCE WINDS EXNTED 40 MILES TO S AND W AND 60 MI
TO N AND E. MINIMUM 700 MB HT 8430 FEET. MIN XTP SLP 941 MBS.
11 DEG TEMP RISE IN CENTER. RADAR COVERAGE FEASIBLE. MANY LAYERS
OF CLOUDS IN EYE.

Figure 1. Microfilm copy of aircraft reconnaissance obtained during Hurricane Donna (1960).

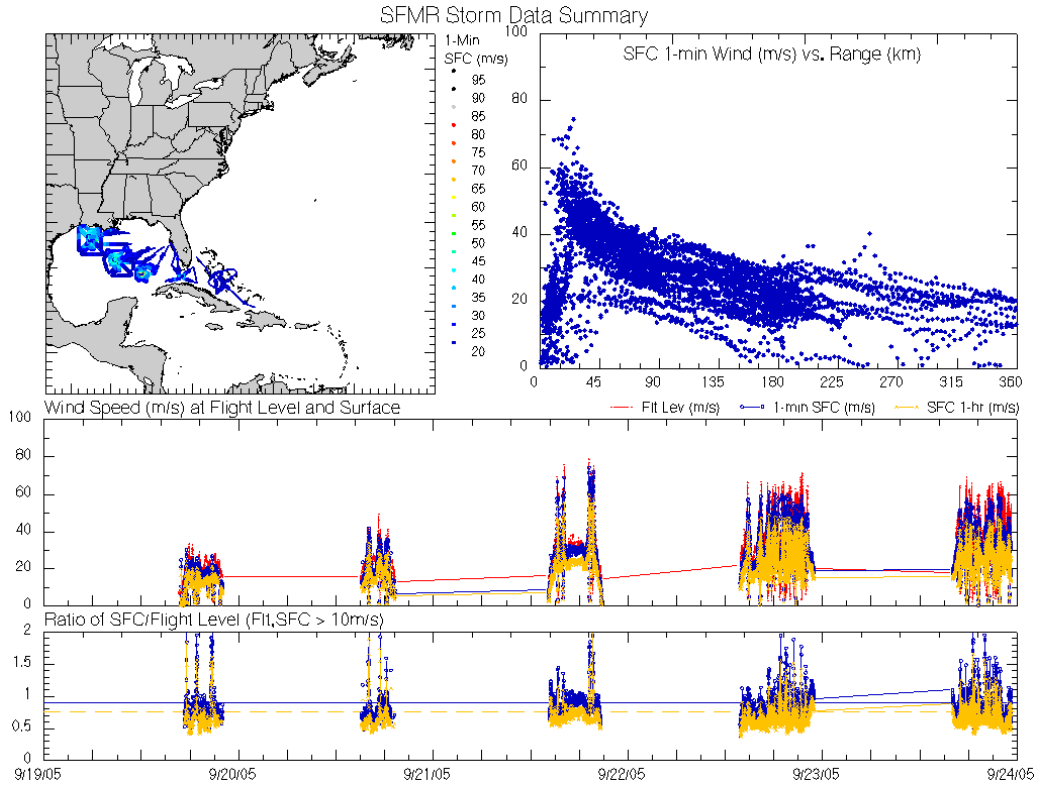

Figure 2. Example summary of Stepped Frequency Microwave Radiometer observations during Hurricane Rita (2005). Geographic locations of the observations are shown in the upper left; 1-minute surface wind vs. range to storm center is shown in upper right; and flight level, surface and 30-minute wind speeds along with their respective ratios vs. time are shown in the bottom figure.

2.2.5 Surface Wind Estimates from the Stepped Frequency Microwave Radiometer

The Stepped Frequency Microwave Radiometer (SFMR), which estimates surface wind speeds, has been in use on HRD aircraft since 1998. The SFMR provides a unique dataset because of its coverage of storms to a degree not available from either point wind estimates from Global Positioning System (GPS) dropwindsondes or occasional direct tropical cyclone encounters with in situ measurement stations. Recently, the entire SFMR archive was reprocessed using a new wind speed retrieval algorithm (Uhlhorn et al., 2007) and made available by HRD. Most storms within the archive have data from multiple missions. A summary of SFMR measurements during Hurricane Rita (2005) is shown in Figure 2.

Wind speeds retrieved from the SFMR have been extensively validated using GPS dropwindsonde data and are believed to represent the peak 1-minute wind at a 10-m reference height. In order to compare SFMR estimates with output from the TropPBL model, a conversion to a 30-minute average wind is required. The Engineering Sciences Data Unit (ESDU) hurricane gust factor algorithm, as discussed in Vickery and Skerlj (2005), is applied to the median of SFMR observations every 30 seconds +/-15 seconds from the source data. The median filter is applied to reduce sampling variability and remove spikes in the dataset. The median filter was not able to remove large spikes apparently caused when the SFMR beam was contaminated by land. A land removal algorithm was developed where observations within 30 seconds of exiting or entering land were removed from the archive. The validity of the assertion that SFMR wind speeds represent peak 1-minute winds at 10-m reference was tested by Cox and Cardone (2007) who compared collocated SFMR and NOAA data-buoy wind speeds. After the process described above was applied to transform SFMR wind speeds to 30-minute average, good agreement was found between the buoy winds and SFMR winds. That study tends to confirm the commonly accepted interpretation of SFMR wind speeds.

2.2.6 Hurricane Track and Intensity

Hurricane track and intensity data were used from updated Atlantic basin hurricane database files (HURDAT) which include the latest results of the Hurricane Reanalysis effort (Landsea et al., 2004 and 2008) for storms up to 1921. Additional track and intensity data came from various National Weather Service (NWS) reports, NHC post-storm reports, Monthly Weather Review annual summaries, and published papers on individual storms.

While the modern portion of HURDAT provides central pressures, much of the early storm data only provides an estimate of the maximum winds. In order to derive an estimate of the central pressure, the Knaff and Zehr (2007) wind-pressure relationship was applied. This technique requires the use of NRA wind and pressure data to derive both the far-field pressure as well as calculate a storm-size parameter. Systems before the availability of NRA data (1900–1947) used the RDA pressure archive and a climatological storm size parameter. For this study, that includes two storms— 1938 and 1944.

2.2.7 Additional Tropical Data

- Gridded and image fields of marine surface wind composites from the National Research Division H*Wind analysis available from http://www.aoml.noaa.gov/hrd/data_sub/wind.html
- Hurricane fix data derived from satellite, aircraft and radar observations obtained from NHC
- Post-storm reports from NOAA, HRD, NHC, and Monthly Weather Review
- Radar data at/near landfall
- Satellite visual, infrared and water vapor imagery
- NHC Storm Wallet Data
- Past storm surge studies/reports in RAMPP area

2.3 TROPICAL PLANETARY BOUNDARY LAYER MODEL

This model, first developed into a practical tool in the Ocean Data Gathering Program (ODGP) (Cardone et al., 1976), can provide a fairly complete description of time-space evolution of the surface winds in the boundary layer of a tropical cyclone from the simple model parameters available in historical storms. The model is an application of a theoretical model of the horizontal airflow in the boundary layer of a moving vortex. That model solves, by numerical integration, the vertically averaged equations of motion that govern a boundary layer subject to horizontal and vertical shear stresses. The equations are resolved in a Cartesian coordinate system whose origin translates at constant velocity, V_f, with the storm center of the pressure field associated with the cyclone. Variations in storm intensity and motion are represented by a series of quasi-steady state solutions. The original theoretical formulation of the model is given by Chow (1971).

A similar model was described in the open literature by Shapiro (1983). The version of the model applied in this study is the result of three major upgrades; the first is described by Cardone et al., (1992); the second by Cardone et al. (1994); and the third by Thompson and Cardone (1996). The first upgrade involved mainly replacement of the empirical scaling law by a similarity boundary layer formulation to link the surface drag, surface wind, and the model's vertically averaged velocity components. The second upgrade added spatial resolution and generalized the pressure field specification.

A more complete description of the theoretical development of the model as upgraded is given by Thompson and Cardone (1996). Most recently, modifications to the model PBL physics allow the introduction of a saturation roughness formulation consistent with that found by Powell (2007) as part of the Modeling of Relevant Physics of Sedimentation (MORPHOS) project (MORPHOS, 2009).

The model pressure field is described as the sum of an axially symmetric part and a large-scale pressure field of constant gradient. The symmetric part is described in terms of an exponential pressure profile, which has the following parameters:

$$P(r) = Po + \sum_{i=2}^{n} dp_i e^{-\left(\frac{R_{pi}}{r}\right)^{Bi}}$$

P(r)	pressure at radius r
Po	minimum central pressure
dp	total pressure deficit
e	natural log
Rp	scale radius of exponential pressure profile
B	profile peakedness parameter

B in the formulation above is an additional scaling parameter whose significance was discussed by Holland (1980). This analytical form is also used to explicitly model the storm pressure field for use in the hydrodynamic model.

The model is driven from parameters that are derived from data in historical meteorological records and the ambient pressure field. The entire wind field history is computed from knowledge of the variation of those parameters along the storm track by computing solutions, or so-called "snapshots," on the nested grid as often as is necessary to describe different stages of intensity, and then interpolating the entire history from the snapshots.

The model was validated originally against winds measured in several ODGP storms. It has since been applied to nearly every recent hurricane affecting the U.S. offshore area, all major storms affecting the South China Sea since 1945, and storms affecting many other foreign basins including the Northwest Shelf of Australia, Tasman Sea of New Zealand, Bay of Bengal, Arabian Sea and Caribbean Sea. Comparisons with overwater measurements from buoys and rigs support an accuracy specification of ± 20 degrees in direction and ± 2 m/s in wind speed (1-hour average at 10-m elevation). Many comparisons have been published (see Ross and Cardone, 1978; Cardone and Ross, 1979; Forristall et al., 1977; 1978; 1980; Cardone et al., 1992, Cardone and Grant, 1994). Prior studies (Cardone and Cox, 2009) have shown that the model winds are comparable to the H*Wind objective analysis wind fields when applied in ADCIRC modeling.

As presently formulated, the wind model is free of arbitrary calibration constants, which might link the model to a particular storm type or region. For example, differences in latitude are handled properly in the primitive equation formulation through the Coriolis parameter. The variations in structure between tropical storm types manifest themselves basically in the characteristics of the pressure field of the vortex itself and of the surrounding region. The interaction of a tropical cyclone and its environment, therefore, can be accounted for by a proper specification of the input parameters. The assignable parameters of the planetary boundary layer formulation, namely planetary boundary layer depth and stability, and of the sea surface roughness formulation, can safely be taken from studies performed in the Gulf of Mexico, since tropical cyclones worldwide share a common set of thermodynamic and kinematic constraints.

Inputs to the tropical model are detailed in Table 2 and are typically fitted every 6 hours during the lifecycle of the storm. Additional fit at critical development times (landfall, rapid intensification, structure changes) are also added as needed.

Table 2. Tropical Model Inputs

dtDate%lCYM	Century-Year-Month (UTC)
dtDate%lDHM	Day-Hour-Minute (UTC)
sLat	Latitude (deg)
sLong	Longitude (deg)
sRot	Rotation of solution (typically 0) in degrees +Rot rotates the entire solution clockwise -Rot rotates the entire solution counter-clockwise
lIsSnap	0=Lat/Long/Rot position only <>0 compute snapshot
sEyeLat	Eye Latitude (deg)
sDirec	Direction (to which) the storm is heading (degrees) 0=Storm heading toward the North 90=Storm heading toward the East 180= Storm heading toward the South 270= Storm heading toward the West
sSpeed	Speed of storm translation (knots)
sEyePres	Central pressure (mb)
sSGW	Synoptic steering flow in which the storm is embedded (knots)
sAN1	Direction (from which) of steering flow (met degrees) 0=Winds from the North (wind travels from North to South) 90 = Winds from the East 180 = Winds from the South 270 = Winds from the West
sRad1	Scale pressure radius (Nmi) of inner radii
sRad2	Scale pressure radius (Nmi) of outer radii (optional)
sDpPercent	Percentage (0-100) of pressure drop associated with RAD1
lNumPro	Number of active azimuthally varying B/Pfar profiles (1 to 4)
tAziPro(:)%sAzimuth	Azimuth (deg) for this profile 0= North Azimuth 90= East Azimuth 180= South Azimuth 270= West Azimuth
tAziPro(:)%sB1	Holland's B associated with Rad1 for profile #
tAziPro(:)%sPFar	Far field pressure (mb) associated with profile #
tAziPro(:)%sB2	Holland's B associated with Rad2 for profile #

2.4 STORM SELECTION FOR SYNOPTIC CLIMATOLOGY

Storm selection for the FEMA Region II study area characterization posed some unique constraints from traditional tropical storm selection for surge response studies. In typical storm selection, the storms with the maximum possible impact/surge generation are selected for hindcast. While direct impact storms are important selection criteria for the study area characterization, it was equally important to select storms of differing track paths and storms with enough in situ and aircraft data to diagnose the shape and deformation of the wind and pressure fields during the lifecycle of the storm.

The initial storm selection regions are three latitude bands from 38°–42° N which represent storms traveling west/inland of the New Jersey–New York coastline, direct hits and storms to the east of the study area (Figure 3). The maximum extents of the western and eastern boundaries were taken from the extent of past studies in New York and New Jersey with an additional buffer. A search of HURDAT tracks from 1900–2009 yielded a storm population of 235 events. Storm data summary plots were generated for each system to evaluate the available in situ and aircraft data available in digital form for storm analysis. Figure 4 illustrates the three main "eras" of tropical data. Data from the early period before the 1940s were sparse and had no satellite or aircraft data for profile fits. Aircraft data start in the late 1940s and provide additional data offshore. In situ data from land stations are also available in digital form. Modern storms have a wealth of in situ data from land stations, coastal stations, and buoys as well as near-continuous monitoring from aircraft.

Storms were reviewed on an individual basis to form a population that represented storms from each of the capture regions (West, Direct and East) that had enough data for wind/pressure profile fits, and were strong enough to create moderate wave/surge response. Nearly all storms before the 1950s were rejected for lack of data except for two notable cases. The September 1938 and 1944 hurricanes both directly affected the New York–New Jersey region and have been the subject of numerous studies and reports that contain data not available in digital form. The 1975 Storm Surge report by Pore and Barrientos (1976) is an essential data source for these storms. Thus, both systems are contained within the storm characterization. An intensity threshold of 980 mb in the Direct and East latitude bands, and 990 mb in the West latitude band was applied to eliminate the weaker storms. Intensity thresholds were applied to restrict the number of systems to be analyzed to a manageable level while retaining a reasonable distribution of systems from each predefined area. The selected intensity thresholds captured all the tropical events identified in the storm selection process, detailed in Section 3, which applied measured residual water level data from nine stations on the USEC to identify events. The resultant storm population of 30 storms is detailed in Table 3.

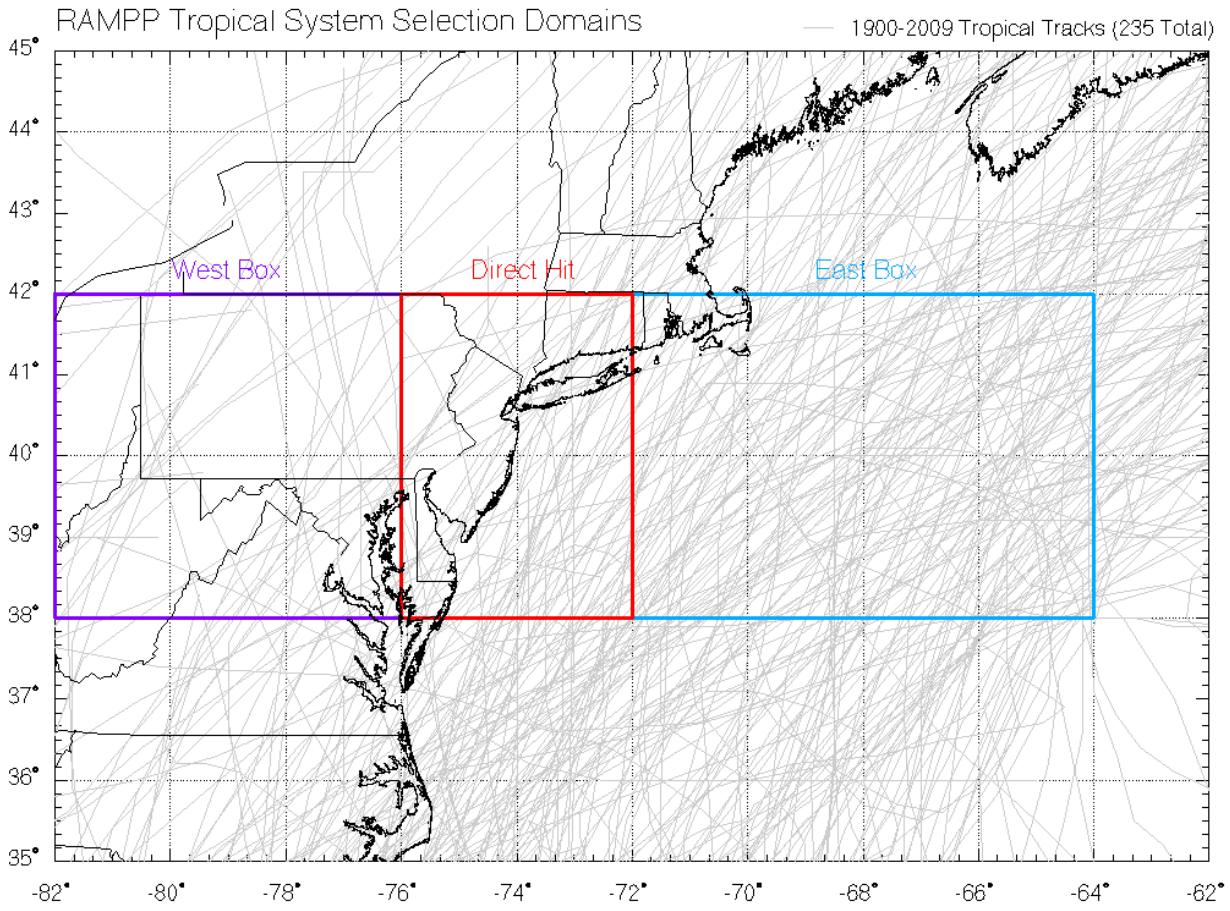

Figure 3. Storm selection capture regions

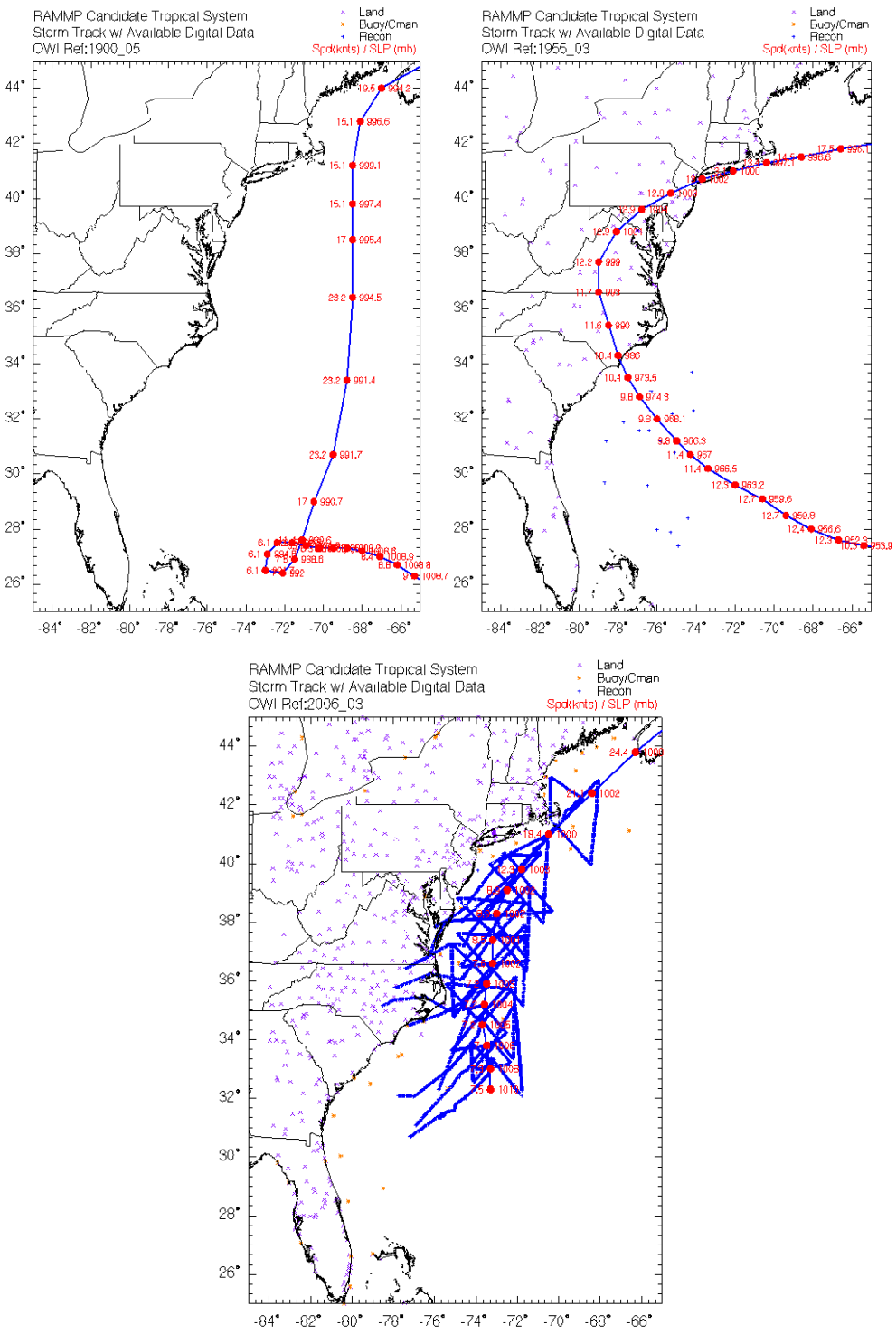

Figure 4. In situ and aircraft data summaries for three tropical systems

Table 3. Selected storms for RAMPP storm characterization

FILE	STORMNAME	CYMDH	MaxWS (1-min kts)	MinSLP (mb)	Box	Track Type
1938_04	NOTNAMED	193809211700	120	937.0	Direct	Ocean Direct
1944_07	NOTNAMED	194409142000	105	952.7	Direct	Ocean Direct
1948_03	NOTNAMED	194809010300	80	979.5	EastBox	Offshore
1952_03	BAKER	195209070600	100	961.5	EastBox	Offshore
1953_02	BARBARA	195308141800	90	970.0	Direct	Coastal/Offshore
1953_04	CAROL	195309070400	90	971.0	EastBox	Offshore
1954_03	CAROL	195408310800	100	962.3	Direct	Ocean Direct
1954_05	EDNA	195409111200	110	947.0	Direct	Ocean Direct
1954_09	HAZEL	195410152000	75	984.0	WestBox	Inland
1955_02	CONNIE	195508130700	85	976.4	Direct	Inland
1958_04	DAISY	195808290600	90	969.3	Direct	Offshore
1960_05	DONNA	196009121400	95	962.5	Direct	Coastal Direct
1961_05	ESTHER	196109210100	90	968.7	Direct	Recurving/Loop
1967_04	DORIA	196709141800	85	976.0	EastBox	Recurving/Loop
1969_07	GERDA	196909091300	85	975.0	EastBox	Offshore
1972_02	AGNES	197206221200	80	977.0	Direct	Coastal Direct
1976_03	BELLE	197608092200	85	974.7	Direct	Ocean Direct
1978_06	ELLA	197809040600	100	961.2	EastBox	Offshore
1985_07	GLORIA	198509271200	110	951.0	Direct	Coastal Direct
1990_02	BERTHA	199007311000	85	973.4	EastBox	Offshore
1991_02	BOB	199108191000	105	952.0	Direct	Ocean Direct
1993_05	EMILY	199309011700	95	966.1	EastBox	Offshore
1996_05	EDOUARD	199609012100	100	961.8	EastBox	Offshore
1996_08	HORTENSE	199609141100	100	959.7	EastBox	Offshore
1999_06	FLOYD	199909161800	75	982.0	Direct	Coastal Direct
2002_08	GUSTAV	200209111200	95	965.2	EastBox	Coastal Offshore
2003_09	ISABEL	200309190500	75	984.4	WestBox	Inland
2004_01	ALEX	200408042000	105	957.0	EastBox	Coastal Offshore
2007_16	NOEL	200711031600	95	967.0	EastBox	Offshore
2009_03	BILL	200908230000	100	961.5	EastBox	Offshore

2.5 TROPICAL SYSTEM ANALYSIS

Given the meteorological data, the tropical system analysis process begins with an intensive reanalysis of the basic hurricane properties including the eye, track, and time history of central pressure, and then develops fits to the radial pressure profile and the ambient pressure field in each storm quadrant. The time histories of entire storm properties are specified within the entire

period to be hindcast and are used to drive a numerical primitive equation model of the cyclone planetary boundary layer to generate a preliminary picture of the time-varying wind field associated with the cyclone circulation itself. That solution is then compared to time histories of accurately measured surface winds (adjusted to standard height) at available measurement sites, and if necessary the model initializations are varied and the solution iterated within the range of natural uncertainties.

A TAWS was developed by Cox and Cardone (2007) to allow a much more accurate and complex diagnosis of the inner core wind field and pressure field distributions. The objective fitting of the radial pressure distribution (either individual legs or azimuthally averaged) to flight-level and in situ data is based on the cost function of Willoughby and Rahn (2006), which was initially formulated to apply only to flight level tangential wind speeds and later extended to a sectionally continuous wind profile with two peaks allowed.

$$S^2 = \sum_{k=1}^{K} \{[v_o(r_k) - v_g(r_k, B)]^2 + g[z_o(r_k) - z(r_k, B)]^2 L_z^{-1}\}$$

Where

S^2	Quadratic cost function computed over radii K
V_o	Observed flight level tangential wind at radius k
V_g	Computed gradient wind at radius k (a function of Holland B)
r	Radius
B	Holland (1980) B parameter
g	Gravity
z_o	Observed geopotential height
z	Computed geopotential height
L_z	Lagrange multiplier

This cost function attempts to minimize the difference between the computed gradient wind (V_g) and observed flight level wind (V_o), and scaled difference in the computed heights z and flight level heights (z_o), in order to determine B given a radius of maximum winds (RMW) estimated from the flight data with the best fit.

In TAWS, the double exponential pressure profile is used to fit the aircraft data much in the same way proposed by Willoughby and Rahn (2006) with the following enhancements: (1) the gradient wind is computed from the surface pressure parameters, rather than the cyclostrophic wind from aircraft heights; (2) Willoughby's cost function has been expanded to allow the use of surface pressure measurements either derived from the aircraft heights (hydrostatically computed from flight level to the surface) or from in situ measurements such as buoys, C-MAN stations, land stations and ship reports; (3) rather than rely on a purely objective determination of Rp1 and

Rp2, an analyst may use the workstation fitting capability iteratively to achieve a best fit based not only on a given snapshot, but considering adjacent snapshots to impose good time-continuity in the results.

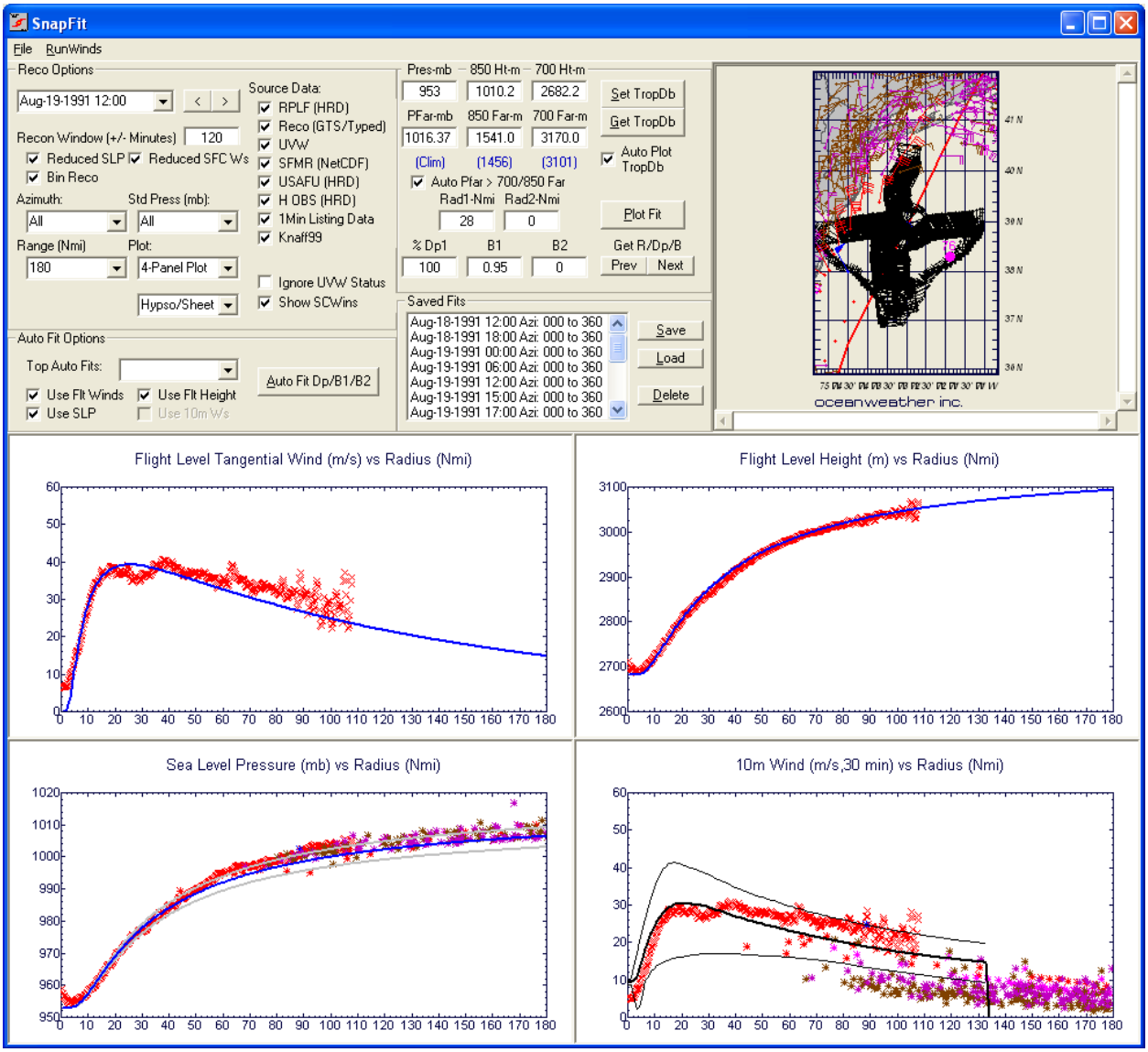

Figure 5. Tropical Analyst Workstation – parameter fit valid Aug-19-1991 12:00 UTC during 1991_02 (Hurricane Bob)

Figure 5 shows the TAWS analysis in 1991_02 (Hurricane Bob). This snapshot of Bob just offshore from New Jersey shows the fit using an inner scale pressure radius of 28 Nmi and no outer scale radius. The lower left panel of the display shows the fitted pressure profile to aircraft derived and in situ pressure measurements after they are azimuthally averaged and composited over +/-120 minutes of the indicated snap time, while the upper part of the lower left panel of the display shows the resulting fit of the gradient wind speed to flight level wind speeds, again azimuthally averaged and composited. The upper part of the display shows the fitted parameters including the radius parameter, peakedness parameters, the central pressure, the far field

pressure, the allocation of the pressure drop between the exponentials and various housekeeping data. The data composited and fitted are shown on the upper right panel. The lower right panel compares the resulting PBL model solutions and NOAA NHC HWnd (Powell et al., 1998) snapshots, if available, with surface in situ and aircraft SFMR 10-m radial wind speed profiles for the azimuthal average and envelopes of maxima and minima of wind speed. A fit to available data is shown for each storm in Appendix A. A full summary of the main fit parameters (central pressure, radii, B) and resultant model maximum winds and radius of maximum winds by storm is summarized in Appendix B.

2.6 REPRESENTATION OF DOUBLE EXPONENTIAL STORMS AS SINGLES

In the resulting analysis, 44 percent of the storm snapshot parameter fits were made applying a double exponential pressure profile. Most double exponential-type snapshots were required to properly model an "outer shelf" in the wind profile, but a few storms did exhibit secondary wind field maxima equal to or greater than the inner wind maxima. Fitting parameters to apply the double exponential model required the addition of a second scale radius (Rad2), second B parameter (B2) and the percentage of the total pressure drop associated with the inner and outer radii (Dp%). The addition of three new parameters adds to the complexity of describing the storm population using a JPM (Joint Probability Method) and can have serious implications on the number of storms required to run a full modeling set.

A sensitivity study was performed to describe a double exponential storm using just the single exponential radius and B parameter to gauge the amount of information lost in such a simplification. Output wind and pressure fields on the study grids were developed so that an ADCIRC run could be made to assess the response model impact.

Gloria 1985 (1985_07) presents an excellent candidate storm. The storm is part of the study validation set, and had strong double exponential pressure and wind profile offshore. In fact, the outer wind radius was stronger than the inner one offshore. If a single exponential profile could describe Gloria, then other double exponential storms with lesser second maxima or outer shelf structure could be fit with even less error.

Figure 6 (a) shows the double exponential fits valid on Sept-27-1985 at 12:00 and 16:00 UTC as analyzed during the tropical characterization. The fit at 12:00 UTC is a strong double wind profile and applied Rad1/2 of 16 and 72, respectively, with Bs of 1.00 and 1.55. The fit just before landfall at 16:00 UTC applied Rad1/2 of 35 and 80 with Bs of 0.8 and 1.00. The pressure drop associated with the inner profile increased from 58 percent to 85 percent at 16:00 UTC as the outer radii winds dropped faster relative to the inner radii as the storm approached land. Figure 6 (b) shows the resultant single exponential profiles applied when the original double exponential maximum wind and radius of maximum wind (model outputs) are preserved. Source data are not refitted for best fit, but rather the single Rad1 and B parameters are iterated until a wind profile within 1 knot of the maxima and 1 Nmi of the double exponential profile results. Thus, the two primary kinematic properties of the double exponential fit are preserved: maxima and radius, which can only be determined by deriving the parameters for the full double exponential representation and using them to drive the PBL model.

Wind field plots from 12:00 UTC (Figure 7) show a nearly perfect agreement in the wind maxima and radius of maximum winds between the double and single exponential fits. The outer winds in the single representation are ~5 knots low at the 40-knot contour on the right side

of the storm. At landfall, the differences in the outer wind maxima are much smaller since the storm structure itself is less peaked in the outer maxima and is more of the shelf structure seen in most double exponential fit storms (Figure 8).

Simulations of the single and double representation of Hurricane Gloria were made using the ADCIRC modeling system and comparisons made at water level measurement sites. Details on this modeling effort and comparison are detailed in a different report, but the resultant storm surge differences were small enough to justify use of the single exponential profile. All snapshots in the database with a double exponential profile were given a derived single exponential representation and both sets of results were retained in the tropical storm database.

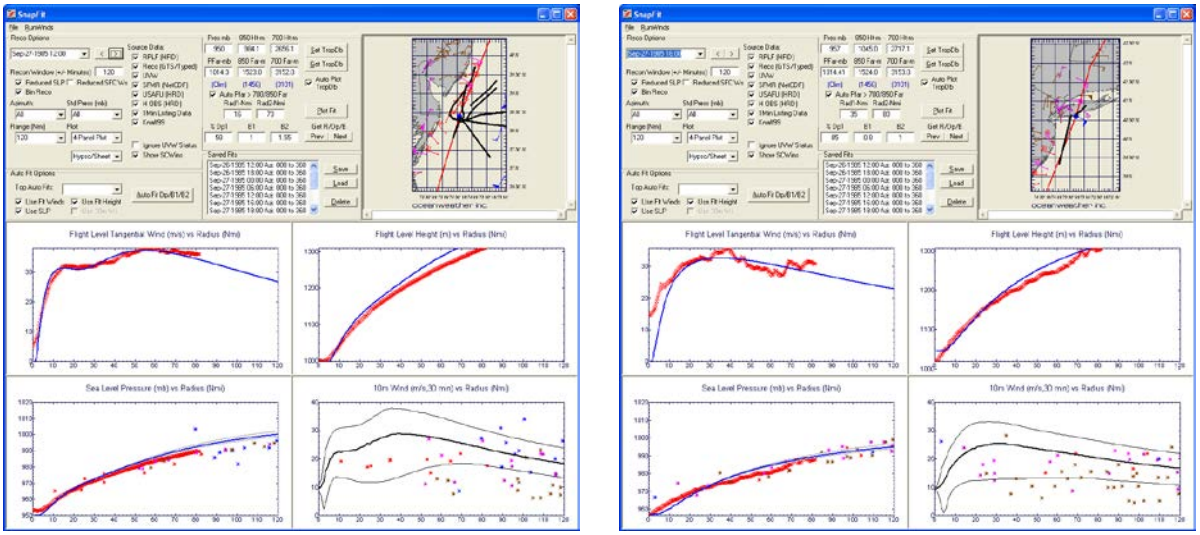

(a)

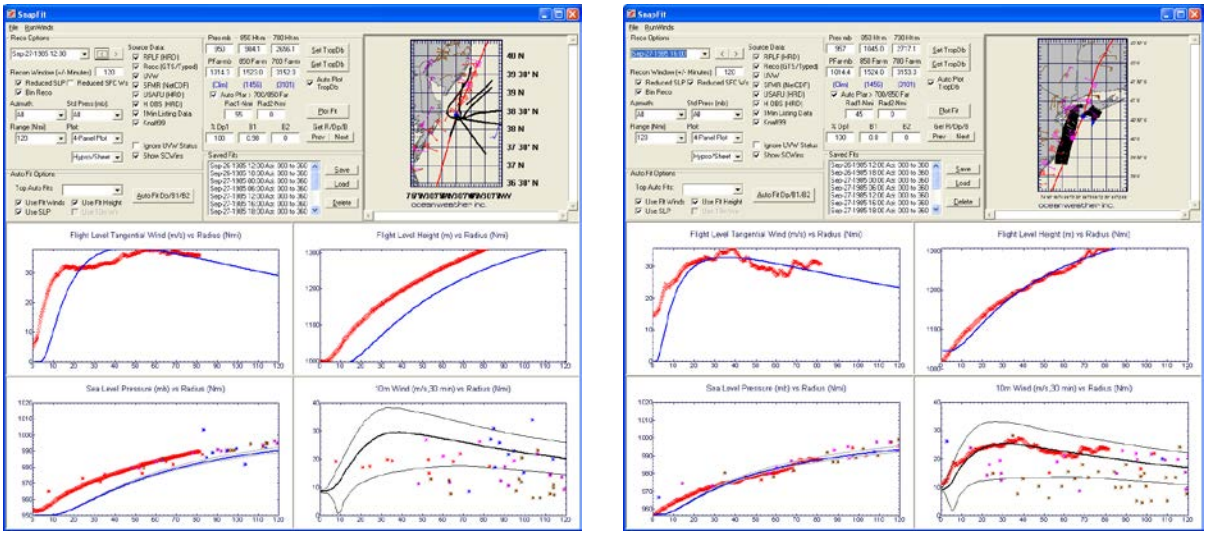

(b)

Figure 6. Double exponential fits (a) and single exponential fits (b) valid Sep27-1985 at 12:00 UTC (left) and 16:00 UTC (right) for Gloria 1985

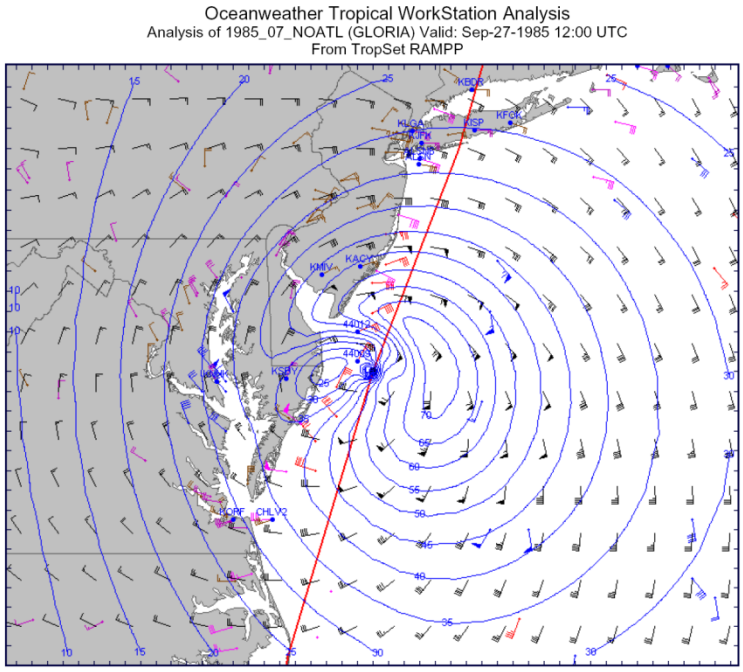

(a)

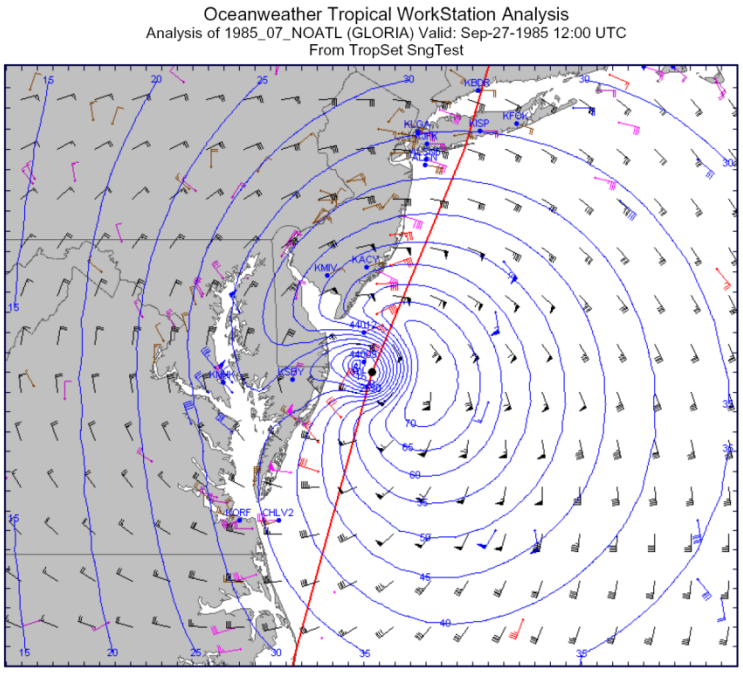

(b)

Figure 7. Resultant 30-minute average wind fields (knots) for the double (a) and single (b) profile fits valid Sep-27-1985 12:00 UTC

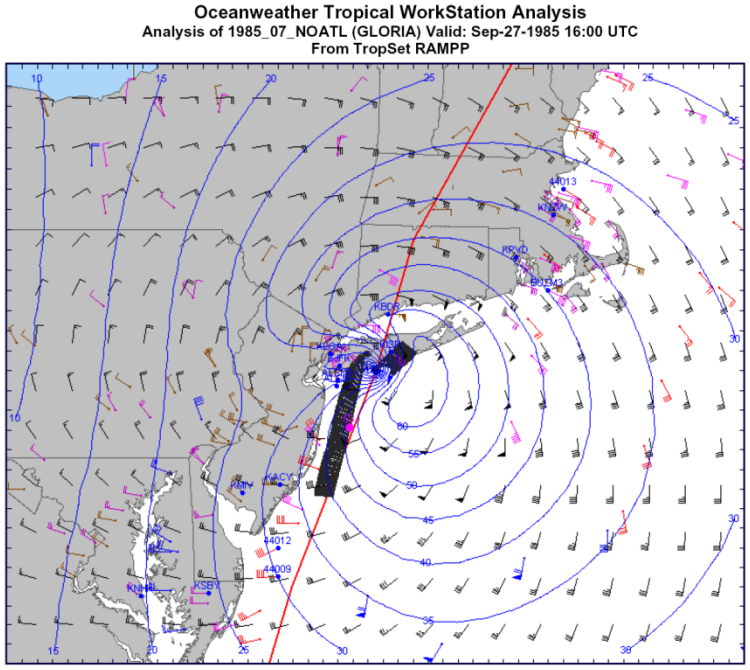

(a)

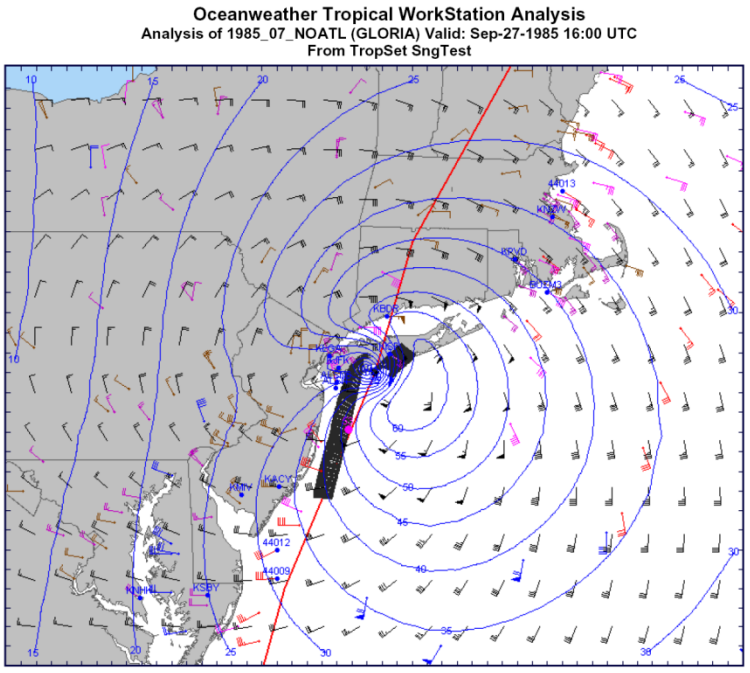

(b)

Figure 8. Resultant 30-minute average wind fields (knots) for the double (a) and single (b) profile fits valid Sep-27-1985 16:00 UTC

2.7 TROPICAL SYSTEM CHARACTERIZATION DATABASE

In all, the population of 30 storms resulted in 420 storm snapshot parameters for use in the study characterization. Concise analyses of the data to highlight interesting features of the database are presented here.

Storms were hindcast in the range of 25°–30° as the southern boundary and to 45°–50° N as the northern boundary. Snapshots are typically fitted every 6 hours with additional 3-hour and landfall positions as required. Central pressures ranged from 912 mb to 1009 mb. Of the 420 snapshots, 185 (44 percent) were identified with a double exponential pressure profile, while the remaining 235 (56 percent) were fitted with a single exponential pressure profile. Snapshots with a double exponential profile were also given a single exponential representation as described in Section 2.6.

Figure 9 shows the regional distribution of snapshots. The first striking result is that almost all systems tend to require either the single or double exponential fit over all the snapshots over water during the period of their history modeled herein. This suggests that factors earlier in the history of this population of storms at lower latitudes have already determined the characteristic internal structure before they recurved northward into the mid-latitudes. Even within the tropics, the processes that determine whether a given tropical cyclone will demonstrate certain patterns are not well understood. The storm may exhibit a classical tight wind profile with a small radius of maximum (say 5–15 Nmi); a well-organized structure with a somewhat larger radius of maximum wind (say 15–30 Nmi); an amorphous shelf-like radial wind profile; or it may oscillate between these states through the eye-wall replacement cycle. Several factors have been implicated such as the mode of formation of a given cyclone (i.e., whether it formed out of a small or large pre-existing disturbance), encounters with land or unfavorable environmental conditions, and whether a given system has undergone several cycles of eye-wall replacement. As a hurricane begins to turn northward, enter the mid-latitudes, gain latitude and accelerate, additional processes come into play that may alter the pre-existing structure.

Another obvious result is that double exponential profile storms tend to rapidly simplify to single exponential with fairly a large radius of maximum wind after landfall such that for strictly overwater snapshots, the allocation of fits between single and double exponential is about 50-50.

Characterization of the peakedness parameters B1 and B2 and scale radius parameters, Rad1 and Rad2, versus central pressure is shown in Figure 10. For the single exponential fitted snapshots (or as noted in the above storms), B tends to scatter as is typical of this parameter, but most of the values lie between 1 and 1.5 with a tendency to increase with added intensity. The scale radius parameter also exhibits typical scatter but with a tendency for small values at increased intensities. This behavior is similar to that exhibited by Gulf of Mexico hurricanes.

For the double exponential fitted snapshots, the inner B values show a tendency for higher values, especially for stronger storms than the B for a single exponential storm (i.e., B1 is markedly higher in storms with double exponential fits). Storm radii continue to show a general trend for stronger storms to have a tighter inner radius as for the population of single exponential storms. Rad2 shows less of a tendency, and overall has more scatter than Rad1. In general, Rad1 is smaller for storms that exhibit a double exponential profile.

Figure 11 shows the percentage of the total pressure deficit associated with Rad1/B1 for snapshot solutions exhibiting a double exponential fit. There is a tendency for the most intense storms to

have a larger percentage associated with the inner Rad1, but the plot shows a high degree of scatter in this association. There appears to be a higher proportion of percentages in the middle range of storm intensities (30–50 percent range) than is seen in the Gulf of Mexico.

In addition to model snapshot parameters, the database also contains an indication of both the amount of data and the quality of the fitted parameters. A subjective skill score from 1 to 3 (best, good, poor) was determined by viewing each snapshot solution with data in the TAWS. For instance, all data in Figure 11 below 935 mb are from the 1944_03 unnamed hurricane. These snapshots were well offshore with little to no data for fits and all received a data fit of 3 (poor). Thus, these fitted parameters should not receive the same kind of weight as a fit with a better skill score. Data and fit results for the 420 snapshots are presented in Table 4.

Table 4. Data and fit counts and percentages determined from the 420 snapshots analyzed

Rating	Data Count	Data %	Fit Count	Fit %
Best (1)	217	51.6	100	23.8
Good (2)	100	23.8	272	64.7
Poor (3)	103	24.5	48	11.4

When the fit and data ratings were plotted with respect to the storm track (Figure 12), a few interesting patterns were detected. Data coverage for storms is generally best when closest to the land station and buoy data along the continental margins, and worst well offshore where little in situ data exist. Profile fits over the oceans and at landfall are generally rated good or best. Fits exhibit an increasing trend of poorer fits as the storms gain latitude and become less tropical in nature. When stratified by month (Figure 13) the best fits all occur in the middle of the tropical season (July-October) with no best fits in June (10 snapshots total) or November (11 snapshots total).

In order to determine if external factors controlled the patterns seen in Figure 12, the data plotted in Figure 12 were stratified by “season” (i.e., pre- and post- September 1 storms) on the notion that summer hurricanes might exhibit “purer” tropical structure than fall hurricanes, but no such behavior was observed. Similarly, relationships were sought only for “high-impact” USEC hurricanes, namely that sub-population of strong tropical systems that moved up and just offshore the USEC, but again no distinct behavior in B1/B2 of R1/R2 was seen. Restriction of the plots only to snapshots for which the fits were judged to be of high quality, as described in the next section, also did not bring out any new systematic differences or reduce the scatter.

A full listing of the 420 snapshot parameters is included in Appendix C: Tropical Characterization Database.

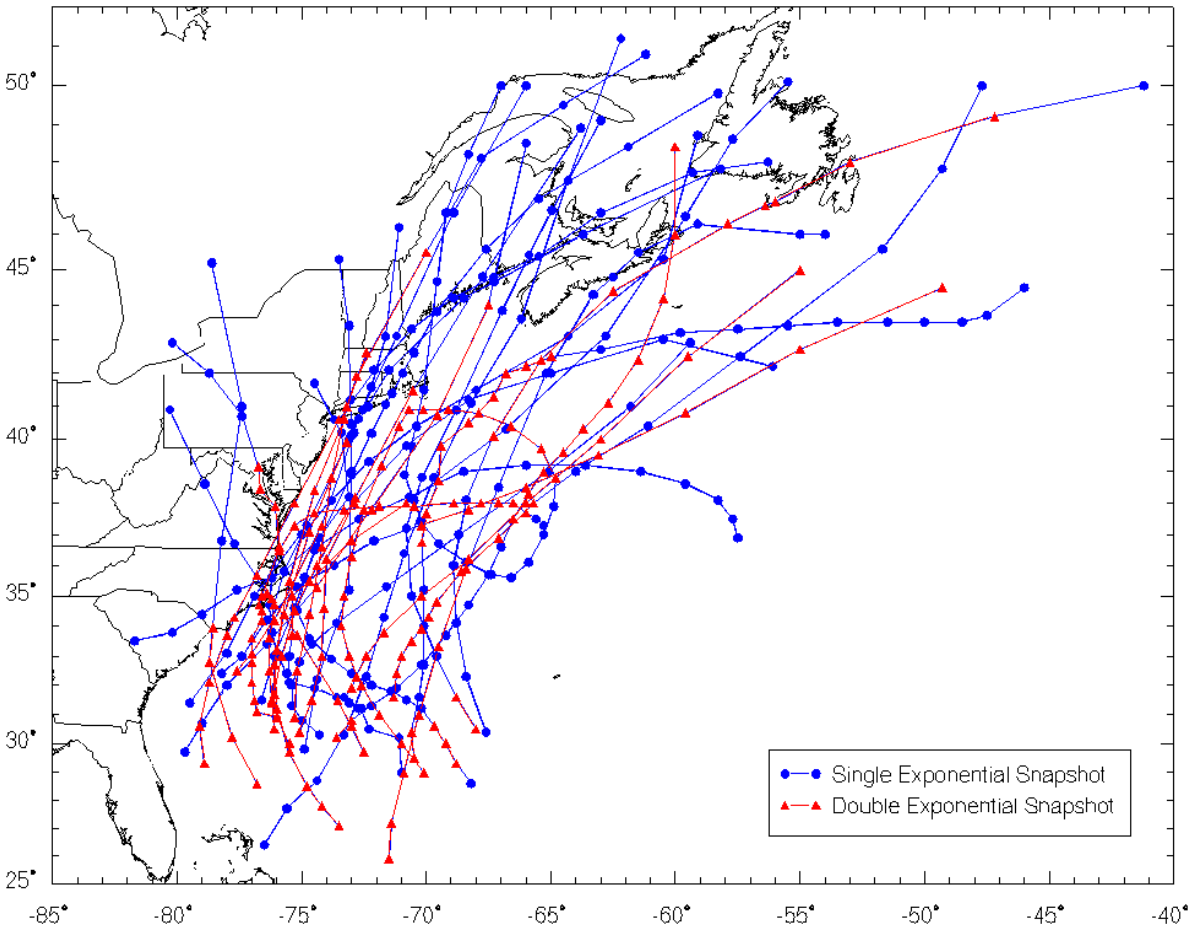

Figure 9. RAMPP snapshots stratified by single (blue) and double (red) exponential fits

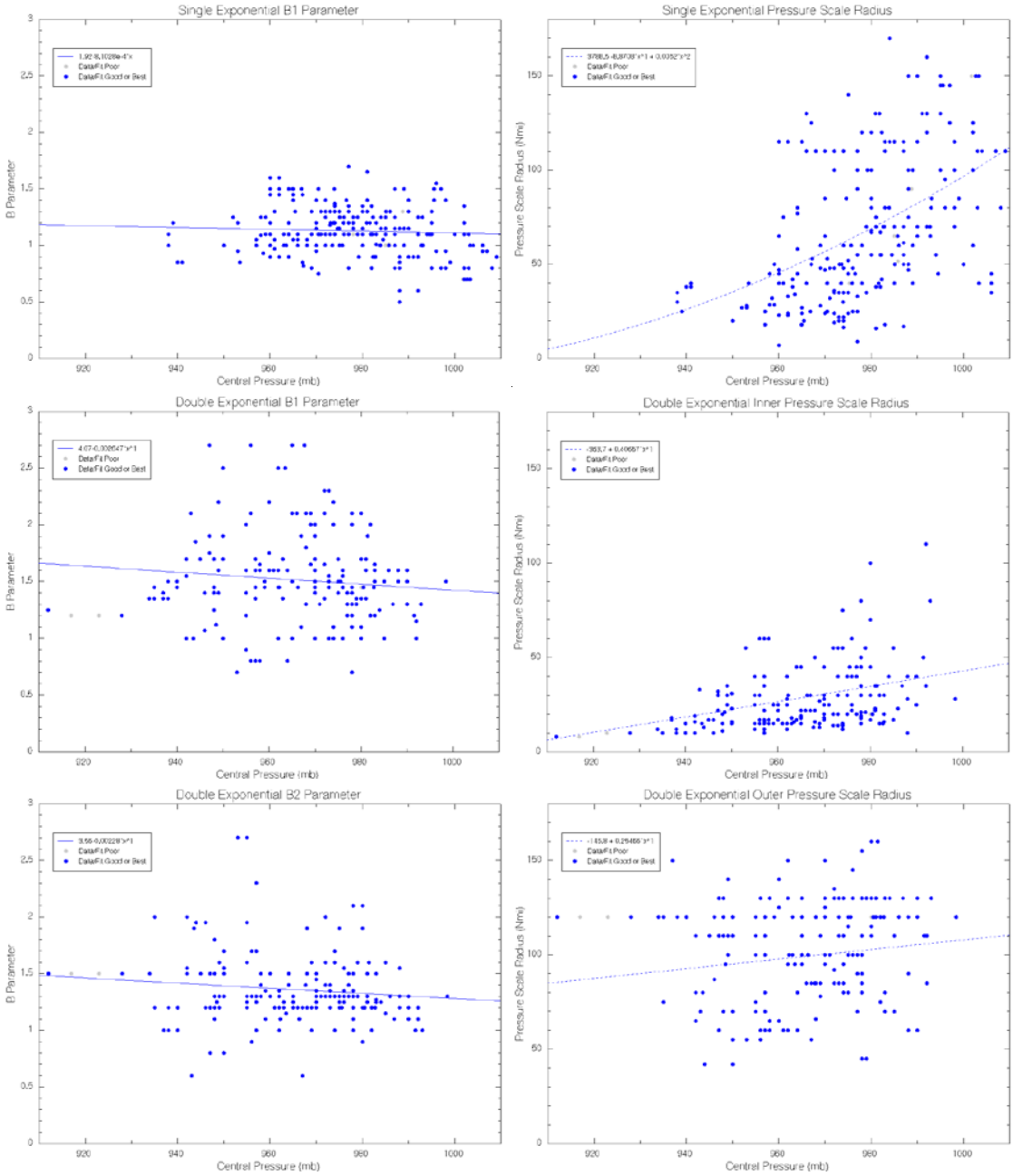

Figure 10. Simple fits to single exponential B1 (top, left) and double exponential B1 (middle, left) and B2 (bottom, left), and fits to scale pressure radius for single exponential (top, right), double exponential inner pressure scale radius (middle, right) and double exponential outer pressure scale radius (bottom, right) from the RAMPP storm snapshot population.

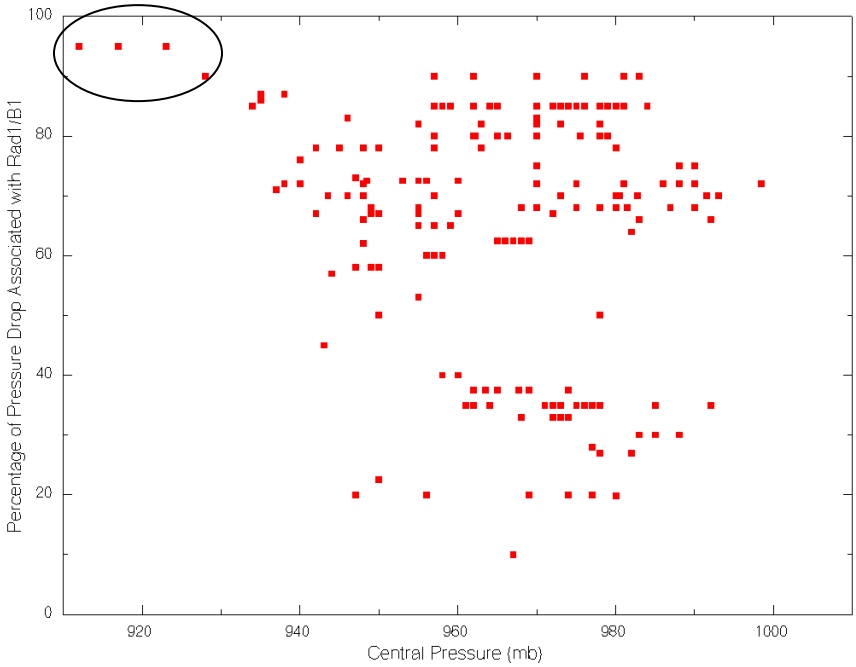

Figure 11. Percentage of pressure drop associated with Rad1/B1 vs. central pressure. All data points less than 935 mb are from the 1944 hurricane.

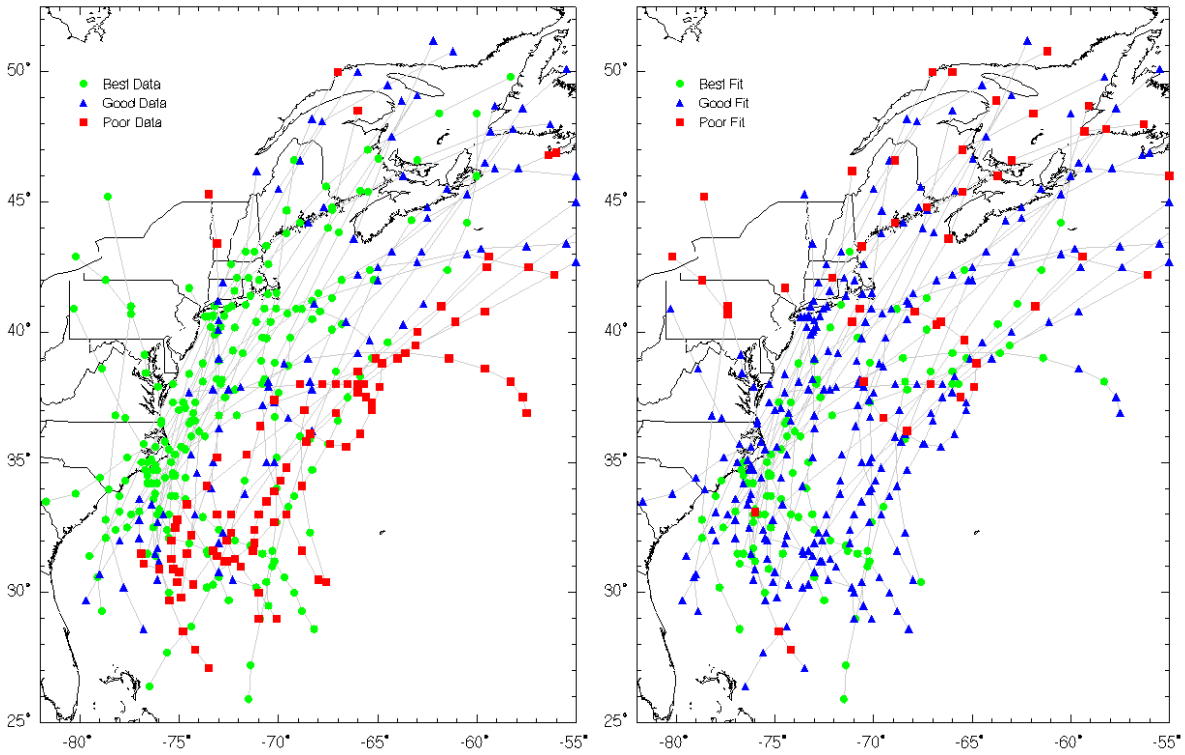

Figure 12. Data (left) and profile fit (right) classifications for all analyzed snapshots

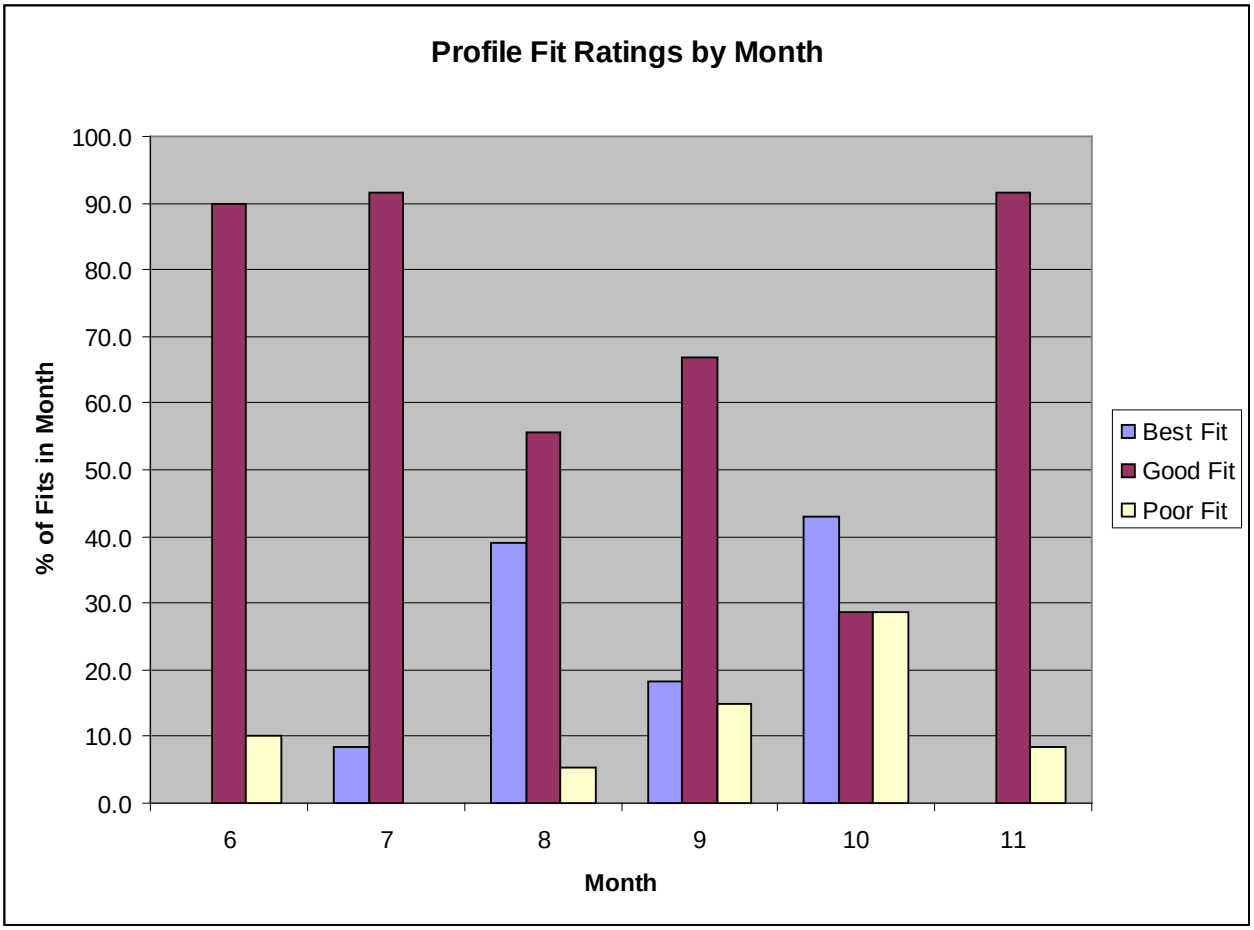

Figure 13. Percentage of profile fit classification by month

SECTION THREE STORM SELECTION

3.1 APPROACH

Storm events were determined based on the measured National Ocean Service (NOS) water level data at nine stations with a long continuous record. The methodology applied is consistent with other recent FEMA studies that were performed in North Carolina and the Chesapeake region. Storm types (Tropical and Extratropical) were divided and ranked separately. A total of 30 extratropical storm events were identified for analysis, while four systems were identified for the tropical calibration/verification phase.

3.2 NOS STATION DATA

Historical NOS water level data are available for download from the NOS website and include both a measured and predicted tide component. The residual (measured- predicted tide) water level was computed for all stations to remove the tidal response so that the storm selections were based on forcing, rather than tidal considerations. Measured data in the study region are shown in Figure 14 and include 20 measurement locations with indicated record periods of at least 15 years. In order to keep the storm selection process as unbiased as possible, multiple long-term records of water level data are required. Stations with large gaps or short time records were not considered. Figure 15 shows the measured residual water level at Chesapeake City, Maryland (NOS station 8573927), for which there are no reports from 1985–2004. When each of the NOS records was examined, nine stations (Figure 16 and Table 5) were found to have good coverage during the period Jan-01-1950 to Nov-30-2009 (present day when the selection was performed).

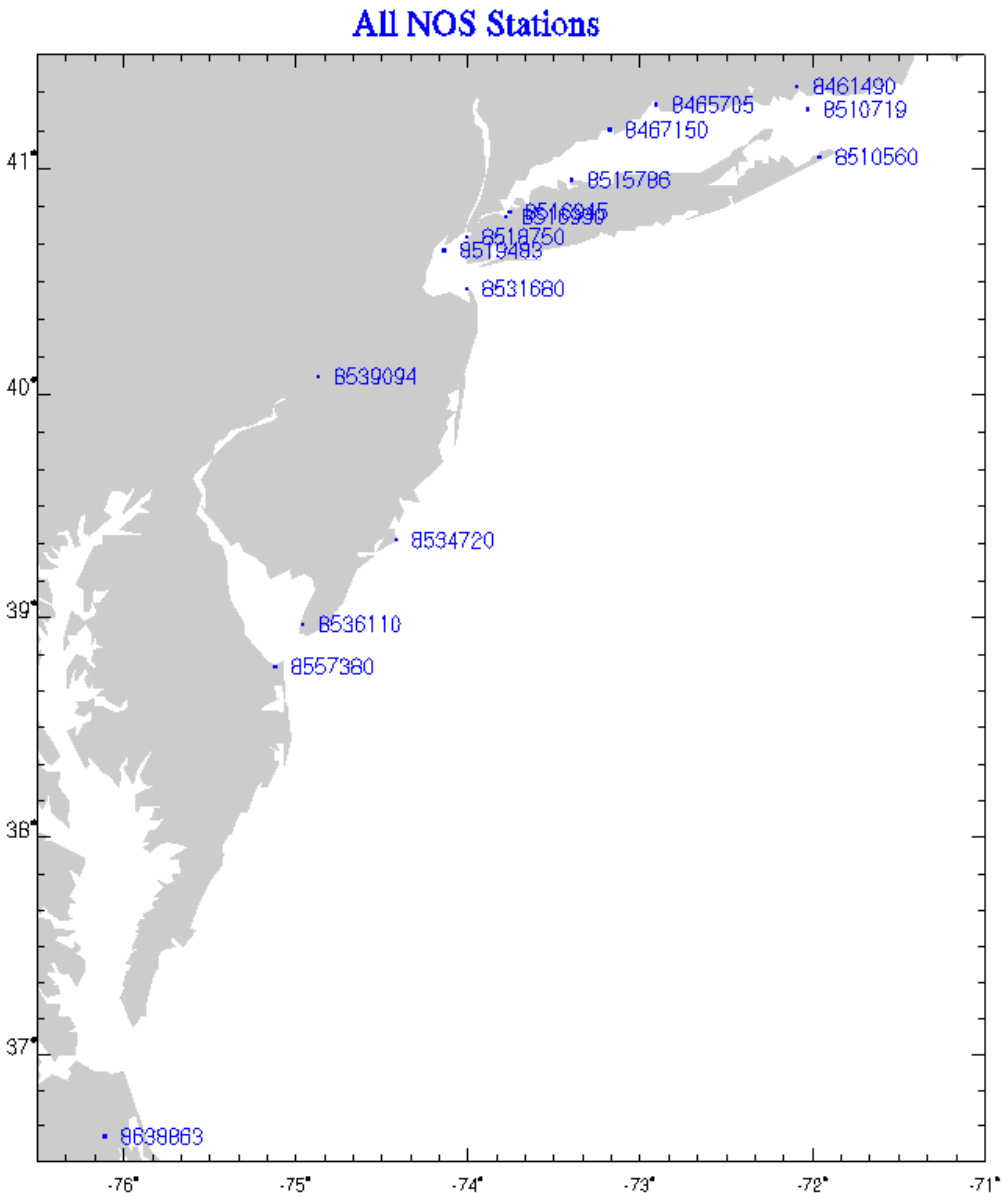

Figure 14. Available NOS station data in study area with record periods of greater than 15 years

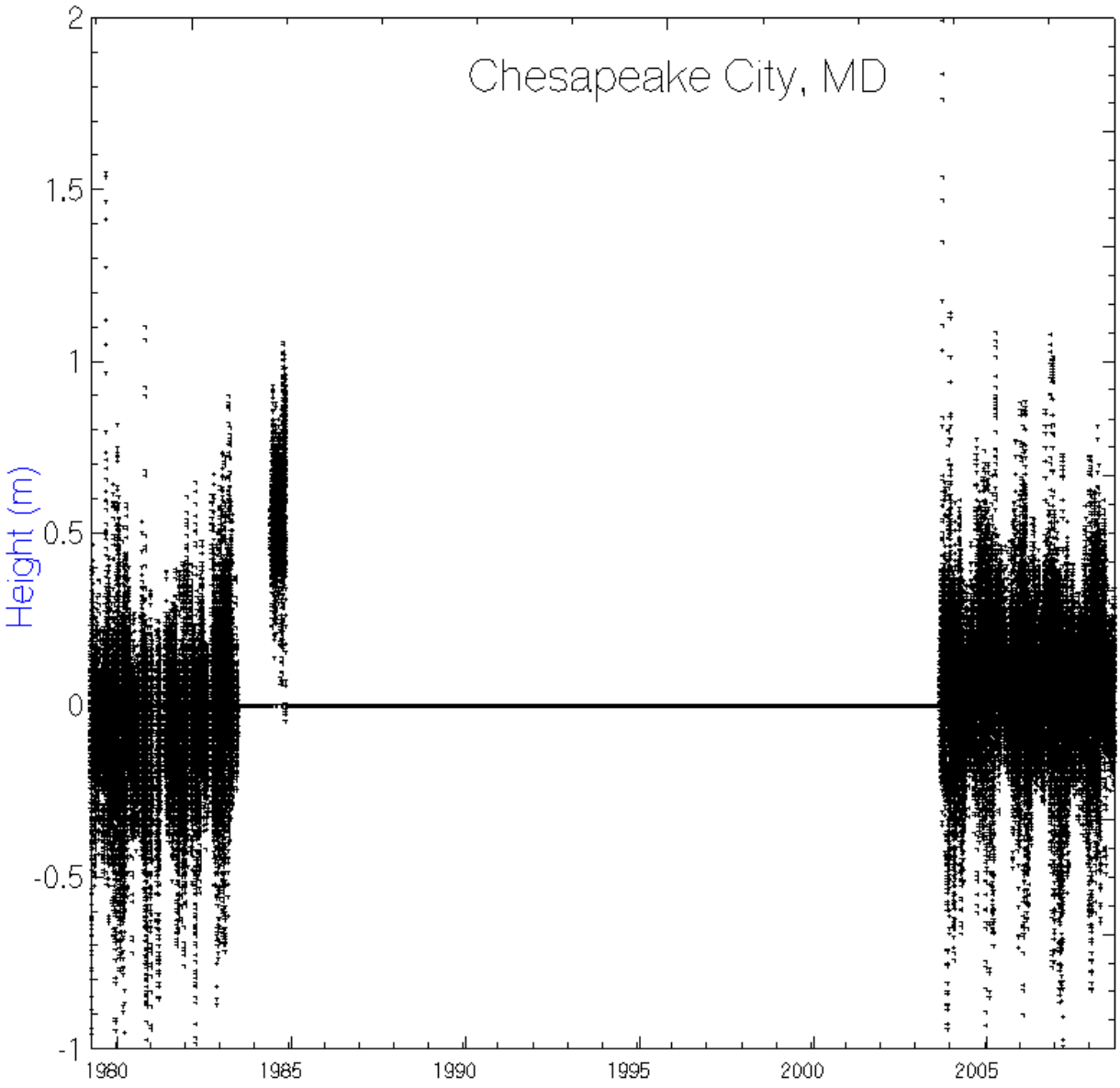

Figure 15. Historical residual water level measurements at Chesapeake City, MD (NOS 8573927) shown as an example of a record with large gaps.

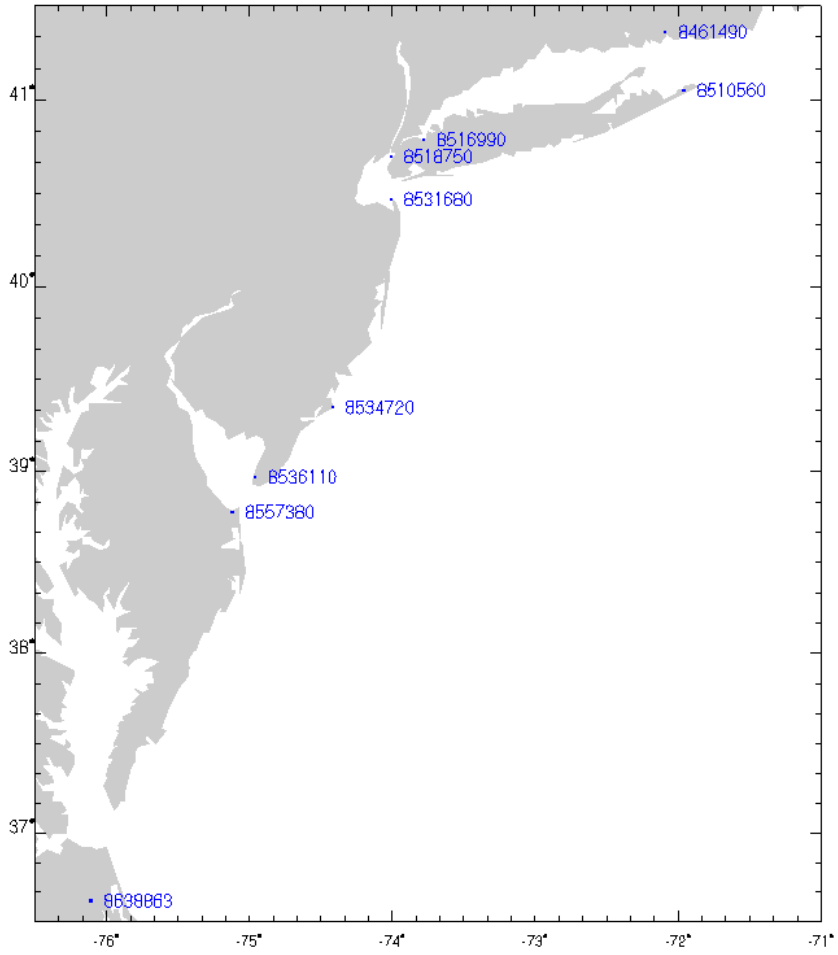

Figure 16. Selected NOS stations applied in the storm selection process

Table 5. Select NOS stations applied in the storm selection process

Station ID	Lat	Long	Record Began (YMD)	Record Ended (YMD)	Station Location
8638863	36.966	-76.113	19750126	20091130	Chesapeake Bay Bridge, VA
8461490	41.36	-72.09	19380601	20091130	New London, CT
8510560	41.05	-71.96	19590101	20091130	Montauk, NY
8516990	40.79	-73.78	19570101	20001130	Willets Point, NY
8518750	40.70	-74.01	19580501	20091130	The Battery, NY
8536110	38.968	-74.96	19651101	20091130	Cape May, NJ
8531680	40.47	-74.01	19100101	20091130	Sandy Hook, NJ
8534720	39.35	-74.42	19110801	20091130	Atlantic City, NJ
8557380	38.782	-75.12	19570101	20091130	Lewes, DE

3.3 STORM RANKING

At each selected NOS station the water level peaks greater than the 99th percentile residual water level were identified individually as candidate storm events. Storm peaks were then ranked by station and the top-ranked events matched with those from the other NOS stations within a 3-day window. A population of 30 events was obtained by taking the top-ranked storms from each NOS station sequentially and removing events found to be tropical in nature as determined by historical tropical storm/hurricane tracks. During this period, the tropical cyclones of Bob (1991), Gloria (1985), Belle (1976), Donna (1960) and Isabel (2003) were identified and removed from the extratropical storm list (Table 6). Multiple storm peaks at a single NOS site within a 3-day period were merged into a single storm event. The storm surge ranked table represents at least the top five measured events at the stations central to the study domain (8557380, 8536110, 8534720, 8531680, 8518750 and 8516990) and top three storms from the peripheral stations (8638863, 8461490 and 8510560). Storms with missing surge values typically indicate that the measured water level was under the 99th percentile threshold, rather than missing from the archive entirely. In all, 30 extratropical events were selected for analysis. Figure 17 illustrates the 30 storms selected as a function of storm rank at The Battery NOS site. This figure illustrates the effectiveness of the 30 storms selected across all the stations at representing the storm population at a single site.

In the tropical storm peaks table (Table 7), hurricanes Gloria (1985) and Donna (1960) are ranked 1 and 2 at most of the central NOS stations and are thus clear candidates for calibration/verification storms. Not shown in Table 7 are the numerous high water marks and data available for the 1938 and 1944 hurricanes as tabulated by Pore and Barrientos (1976). While both storms lack digital data and aircraft data offshore, each storm has a wealth of in situ data (both wind/pressure for forcing and high water estimates) at landfall and both storms are notable for their strength at landfall. Thus, both the 1938 and 1944 events were included in the calibration/verification effort.

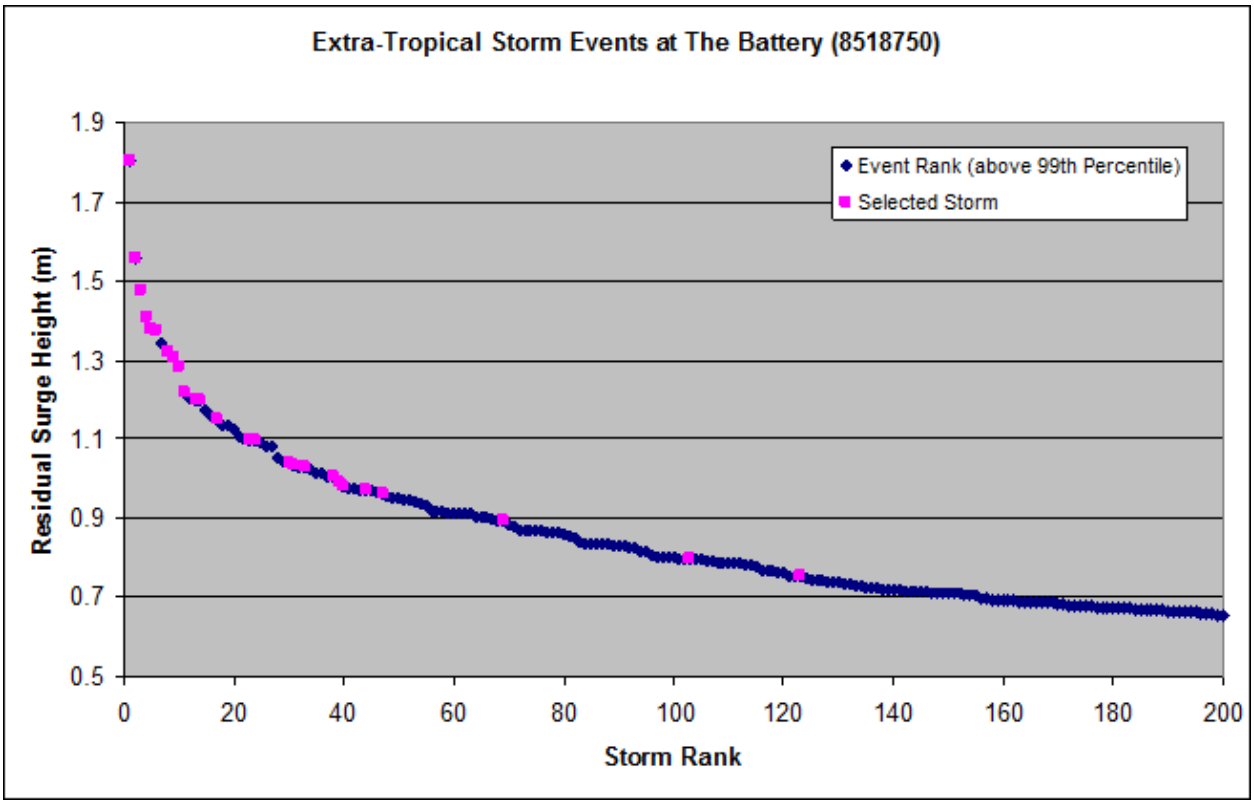

Figure 17. Ranked extratropical residual storm peaks above the 99th percentile with selected storm events at the Battery, NY NOS station.

Table 6. Extratropical storms selected from the period Jan-1950 to Nov-2009 based on 9 NOS stations.

	New London, CT 8461490			Montauk, NY 8510560			Willets Point, NY 8516990			The Battery, NY 8518750			Sandy Hook, NJ 8531680			Atlantic City, NJ 8534720			Cape May, NJ 8536110			Lewes, DE 8557380			Chesapeake Bay Bridge, VA 8638863		
Storm Date	Date	Residual	Rank	Date	Residual	Rank	Date	Residual	Rank	Date	Residual	Rank	Date	Residual	Rank	Date	Residual	Rank	Date	Residual	Rank	Date	Residual	Rank	Date	Residual	Rank
19501125	19501126	1.66	1										19501125	2.40	1												
19610413	19610413	0.70	100				19610413	1.46	17	19610413	1.04	30	19610413	1.18	20							19610413	0.68	125			
19620306	19620307	0.74	74							19620306	1.31	9	19620306	1.36	10	19620306	1.17	4				19620307	1.69	1			
19640112							19640113	1.39	21	19640113	0.97	44	19640109	0.68	188	19640113	1.03	12				19640113	0.99	27			
19660123				19660123	0.95	20				19660123	1.10	23	19660123	1.28	14				19660123	0.98	19						
19681112	19681112	1.18	6	19681112	1.18	6	19681112	1.91	4	19681112	1.32	8	19681112	1.40	8	19681112	1.14	6	19681112	0.93	27						
19701217	19701217	1.02	17	19701217	0.91	26	19701217	1.63	12	19701217	0.99	39	19701217	1.06	35							19701217	0.68	130			
19710208							19710208	2.20	2																		
19711125	19711125	0.75	73	19711125	0.86	42	19711125	1.38	22	19711125	1.20	13	19711125	1.37	9	19711125	0.94	22									
19720219	19720219	1.05	14	19720219	1.12	8	19720219	1.66	11	19720219	0.98	40				19720219	1.26	3				19720219	0.96	31			
19741202	19741202	1.10	9				19741202	1.49	15				19741202	1.66	3	19741202	1.16	5									
19790125	19790125	1.10	10	19790125	1.01	16				19790125	1.38	5	19790125	1.28	13				19790125	0.66	107						
19840329	19840329	1.17	7	19840329	1.25	2	19840329	1.82	7	19840329	1.56	2	19840329	1.63	5				19840329	1.05	10	19840329	1.22	6	19840329	0.74	49
19870123	19870123	1.22	5	19870123	1.10	9	19870123	1.84	6	19870123	1.10	24	19870123	1.19	18	19870122	0.99	17	19870122	0.98	18	19870122	1.12	13	19870122	0.77	41
19911031	19911031	1.16	8	19911031	1.24	3	19911031	1.57	13	19911031	1.41	4	19911031	1.40	7	19911031	1.41	1	19911031	1.08	7	19911031	1.15	11	19911101	0.88	23
19921211	19921211	1.25	3	19921211	1.21	5	19921211	2.25	1	19921211	1.81	1	19921211	2.07	2				19921211	1.34	2	19921211	1.14	12	19921212	0.78	40
19930314	19930314	1.34	2	19930314	1.28	1	19930314	1.85	5	19930313	1.48	3	19930313	1.65	4				19930314	1.02	14	19930313	1.08	15			
19940303	19940303	0.79	64	19940303	0.85	43	19940303	1.23	37	19940303	1.20	14	19940303	1.31	12	19940303	1.04	11	19940303	0.98	20	19940303	1.01	24			
19941224	19941224	1.08	12	19941224	1.16	7	19941224	2.00	3	19941224	1.03	31	19941224	1.15	23				19941224	0.93	28	19941224	0.92	41	19941224	0.75	47
19950204	19950204	1.04	15	19950204	1.01	15	19950204	1.48	16	19950204	0.80	103															
19951115	19951115	0.88	33	19951115	0.87	39	19951115	1.74	9	19951115	1.29	10	19951115	1.32	12	19951114	0.96	20	19951114	0.90	33	19951114	0.91	44			
19960108	19960108	0.97	25	19960108	1.02	13	19960108	1.37	24	19960108	1.37	6				19960108	1.40	2	19960108	1.55	1	19960108	1.52	2			
19961020	19961020	1.02	18				19961020	1.70	10	19961019	1.00	38				19961019	0.71	78	19961019	0.66	104						
19961206	19961206	0.90	28	19961208	0.93	21	19961206	1.31	27	19961206	1.22	11	19961206	1.14	24	19961206	0.83	39	19961206	0.69	94						
19980128							19980128	0.77	158	19980128	0.76	123				19980128	0.80	43	19980128	1.17	5	19980128	1.42	3	19980128	1.37	2
19980205							19980205	1.12	48	19980205	1.03	33	19980205	1.12	30	19980205	1.08	7	19980205	1.32	3				19980205	1.37	3
20051025	20051025	1.03	16	20051025	1.02	12				20051025	1.15	17	20051025	1.20	17	20051025	1.00	16	20051025	1.07	9	20051025	1.10	14	20051025	0.88	22
20070416	20070416	1.22	4	20070416	1.07	10				20070416	0.96	47	20070416	1.01	42	20070416	0.76	57									
20080512													20080512	0.99	46	20080512	0.98	18	20080512	1.03	12	20080512	1.26	5	20080513	1.01	11
20091113										20091114	0.90	69	20091114	1.00	44	20091113	0.89	30	20091113	1.19	4	20091113	1.38	4	20091113	1.66	1

Table 7. Tropical Cyclones identified in storm selection process

	New London, CT 8461490			Montauk, NY 8510560			Willets Point, NY 8516990			The Battery, NY 8518750			Sandy Hook, NJ 8531680			Atlantic City, NJ 8534720			Cape May, NJ 8536110			Lewes, DE 8557380			Chesapeake Bay Bridge, VA 8638863		
Storm Name	Date	Residual	Rank	Date	Residual	Rank	Date	Residual	Rank	Date	Residual	Rank	Date	Residual	Rank	Date	Residual	Rank	Date	Residual	Rank	Date	Residual	Rank	Date	Residual	Rank
Bob	19910819	1.34	3				19910819	1.18	2																		
Gloria	19850927	1.72	2	19850927	1.11	1	19850927	1.66	1	19850927	2.03	1	19850927	2.22	1	19850927	1.44	1	19850927	1.15	1	19850927	1.15	2	19850927	1.10	2
Belle	19760810	0.95	5				19760810	1.18	3	19760810	1.15	3	19760810	1.38	3	19760810	1.04	3									
Donna	19600912	1.30	4	19600912	0.99	2				19600912	1.63	2	19600912	1.54	2	19600912	1.10	2				19600912	1.26	1			
Isabel																20030918	0.72	5				20030919	0.91	3	20030918	1.43	1
Floyd							19990916	0.81	4	19990916	1.10	4	19990916	1.02	4	19990916	0.81	4	19990916	0.75	3	19990916	0.74	5	19990916	0.90	3
Doria																			19670916	0.75	2	19670916	0.87	4			
Agnes										19720622	0.72	5	19720622	0.78	7												
Carol	19540831	1.79	1										19540831	0.81	5												
Connie													19550813	0.78	6												

SECTION FOUR CALIBRATION/VERIFICATION OF TROPICAL AND EXTRATROPICAL ANALYSIS

4.1 APPROACH

Analysis of the tropical systems for the calibration/verification of the modeling system applies the same tropical methodology detailed in Section 1 of this report to determine the required input parameters to drive the tropical PBL model. Wind and pressure fields developed by the PBL model were exported to a series of wind and pressure grids detailed below. For extratropical storms, fields were derived using the kinematic analysis approach, which is detailed in Section 4.3.

Wind fields were developed on two grid systems: a basin grid (WNAT28km) covered the domain 5-47.5N, 98-57.5W at a 0.25-degree latitude-longitude grid with time step of 15 minutes; and a fine grid covered the domain 38.4-41.75N, 75-71W at 0.05-degree latitude-longitude grid with 15-minute time step. All winds are 10-m neutral representing a 30-minute average.

4.2 TROPICAL SYSTEMS

4.2.1 1938 Hurricane

The "Great New England Hurricane" of 1938 made landfall at 19:45 UTC on September 21, 1938, with a central pressure of 941 mb and maximum 1-minute wind speeds of 100-105 knots. The radius of maximum winds at landfall was 30–35 Nmi. Measured residual water levels at the Battery, NY, and Sandy Hook, NJ, were in the range of 3–4 feet, while maximum estimated high water marks were up to 15.7 feet on Long Island according to data compiled by Pore and Barrientos (1976). Figure 18 depicts the storm track and envelope of maximum winds. The track and landfall intensity applied in the hindcast is consistent with Landsea (2008), which displaced the storm track westward of the HURDAT track. This track/intensity also verified well against available wind trace at Hempstead Mitchell Field Air Force Base, as shown in Figure 19.

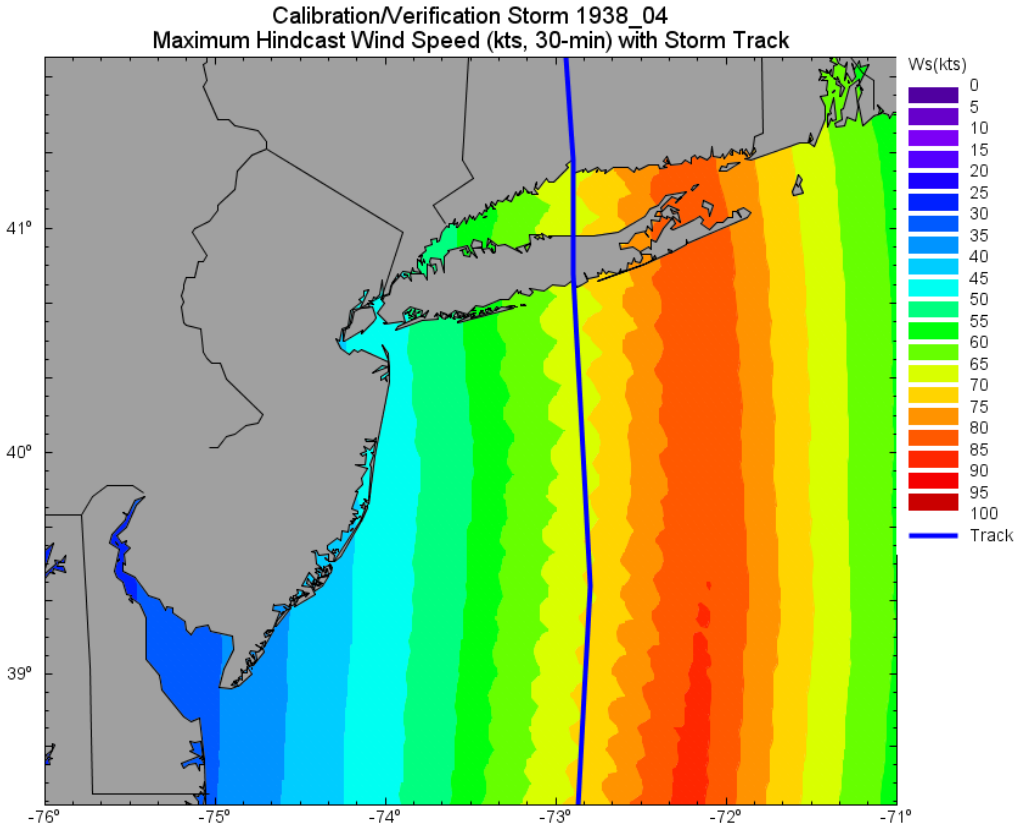

Figure 18. Maximum wind speed envelope (knots, 30-min) during 1938_04.

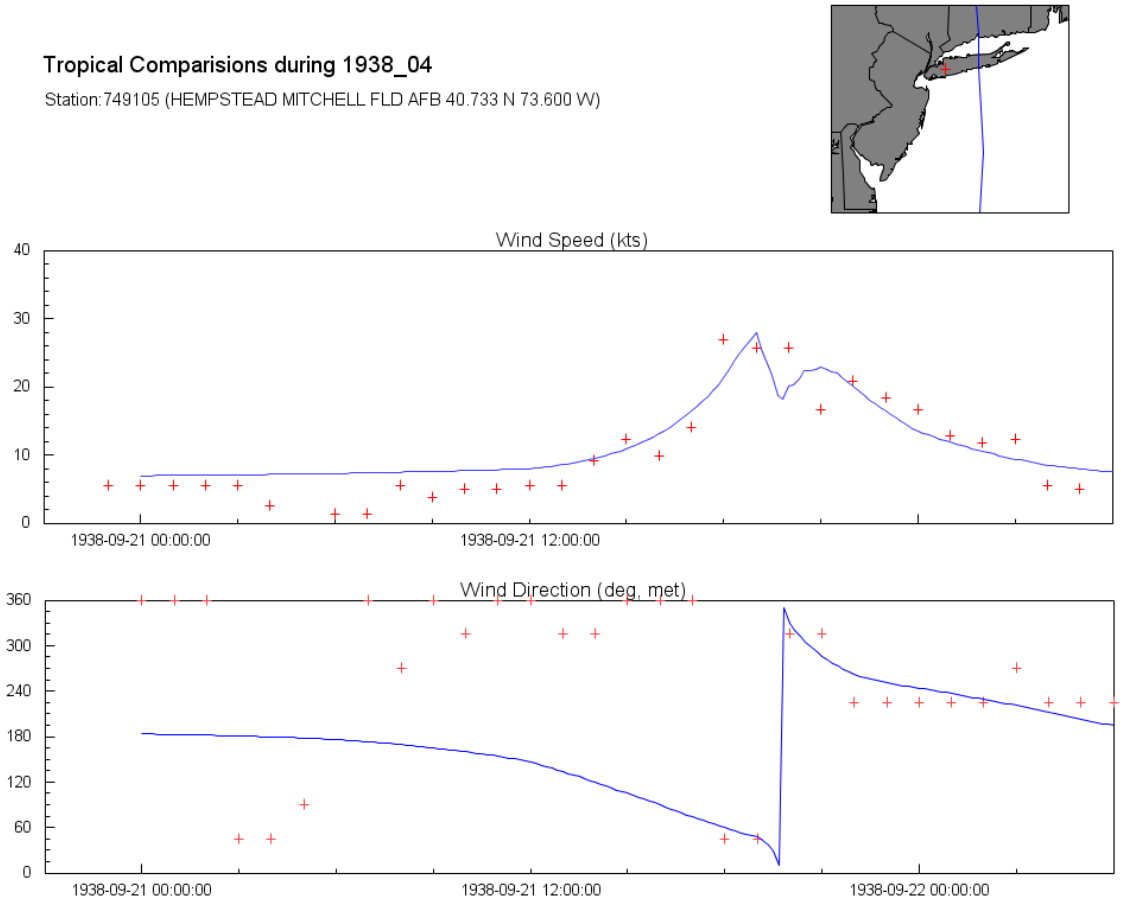

Figure 19. Wind speed and direction comparison at Hempstead Mitchell Field during 1938_04.

4.2.2 1944 Hurricane

The "Great Atlantic Hurricane" of 1944 made landfall at 03:00 UTC on September 15, 1944, with a central pressure of 963 mb and maximum 1-minute wind speeds of 90–95 knots. The radius of maximum winds at landfall was 23–28 Nmi. Measured residual water levels at the Battery, NY, and Sandy Hook, NJ, were in the range of 4–5 feet, while maximum estimated high water marks were up to 10.5 feet according to data compiled by Pore and Barrientos (1976). Figure 20 depicts the storm track and envelope of maximum winds. The wind trace at Hempstead Mitchell Field Air Force Base is shown in Figure 21.

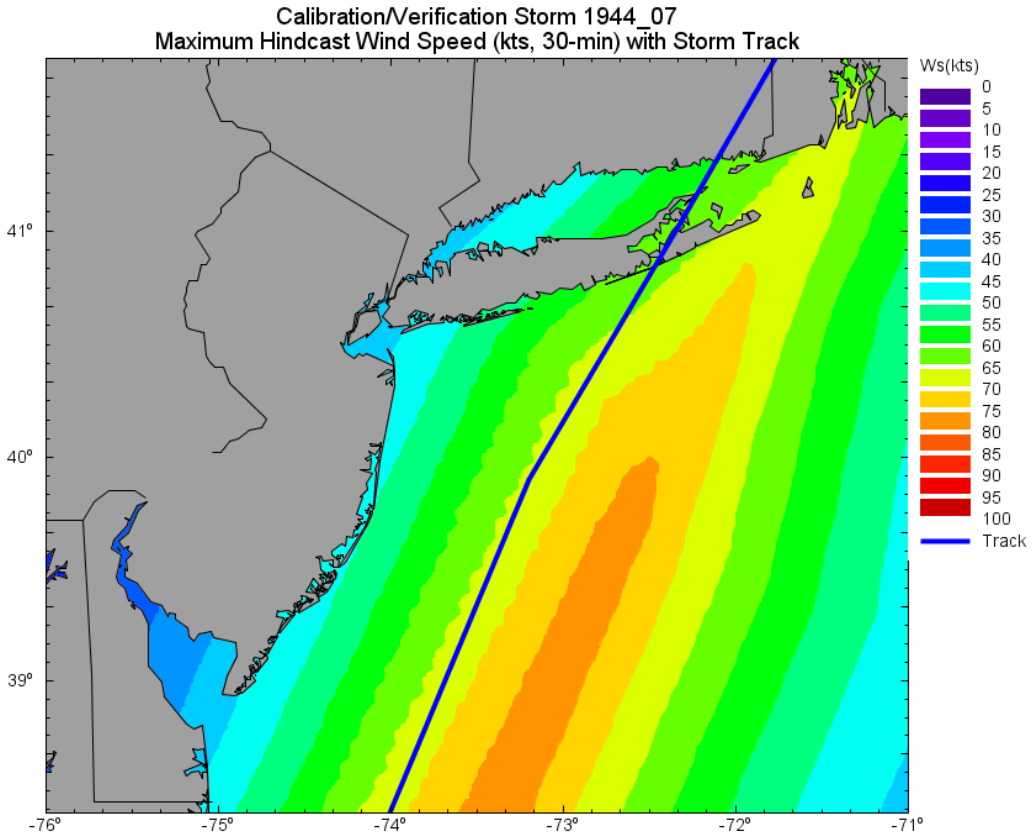

Figure 20. Maximum wind speed envelope (knots, 30-min) during 1944_07.

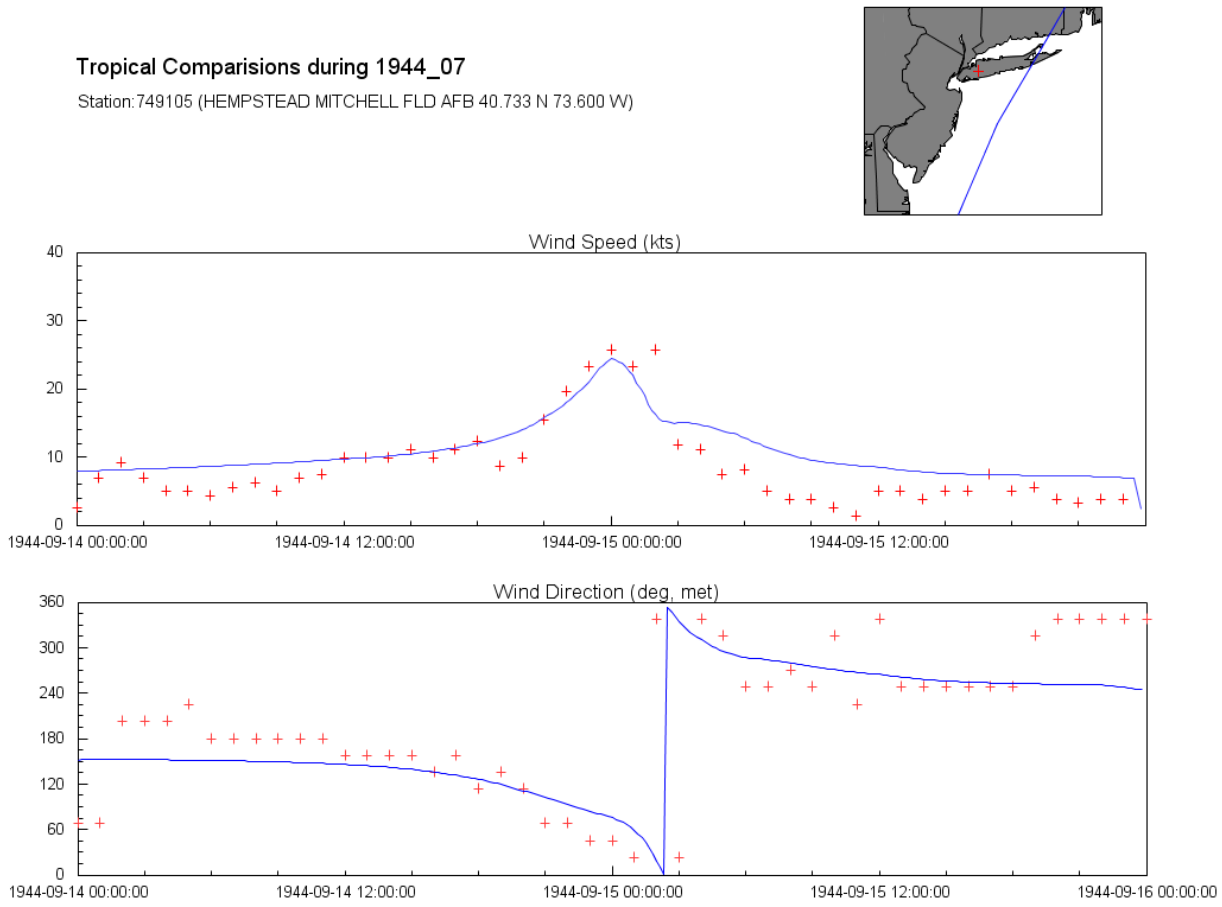

Figure 21. Wind speed and direction comparison at Hempstead Mitchell Field during 1944_07.

4.2.3 Hurricane Donna (1960)

Hurricane Donna of 1960 made landfall at 20:00 UTC on September 12, 1960, with a central pressure of 958 mb and maximum 1-minute wind speeds of 80–85 knots. The radius of maximum winds at landfall was 50–55 Nmi. Tides were reported 5.7 to 6.1 feet above normal according to NWS reports for Atlantic City, NJ, and New York City, NY, respectively. Figure 22 depicts the storm track and envelope of maximum winds. The wind trace at New York's John F. Kennedy Airport is shown in Figure 23.

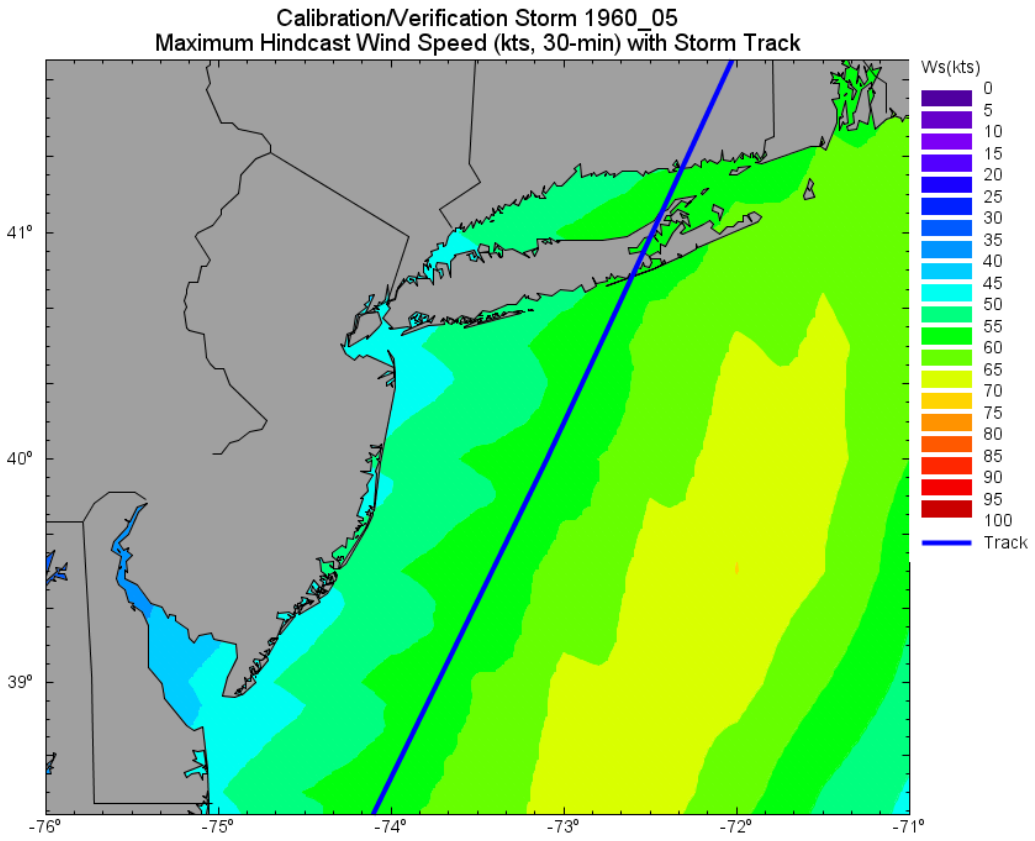

Figure 22. Maximum wind speed envelope (knots, 30-min) during 1960_05.

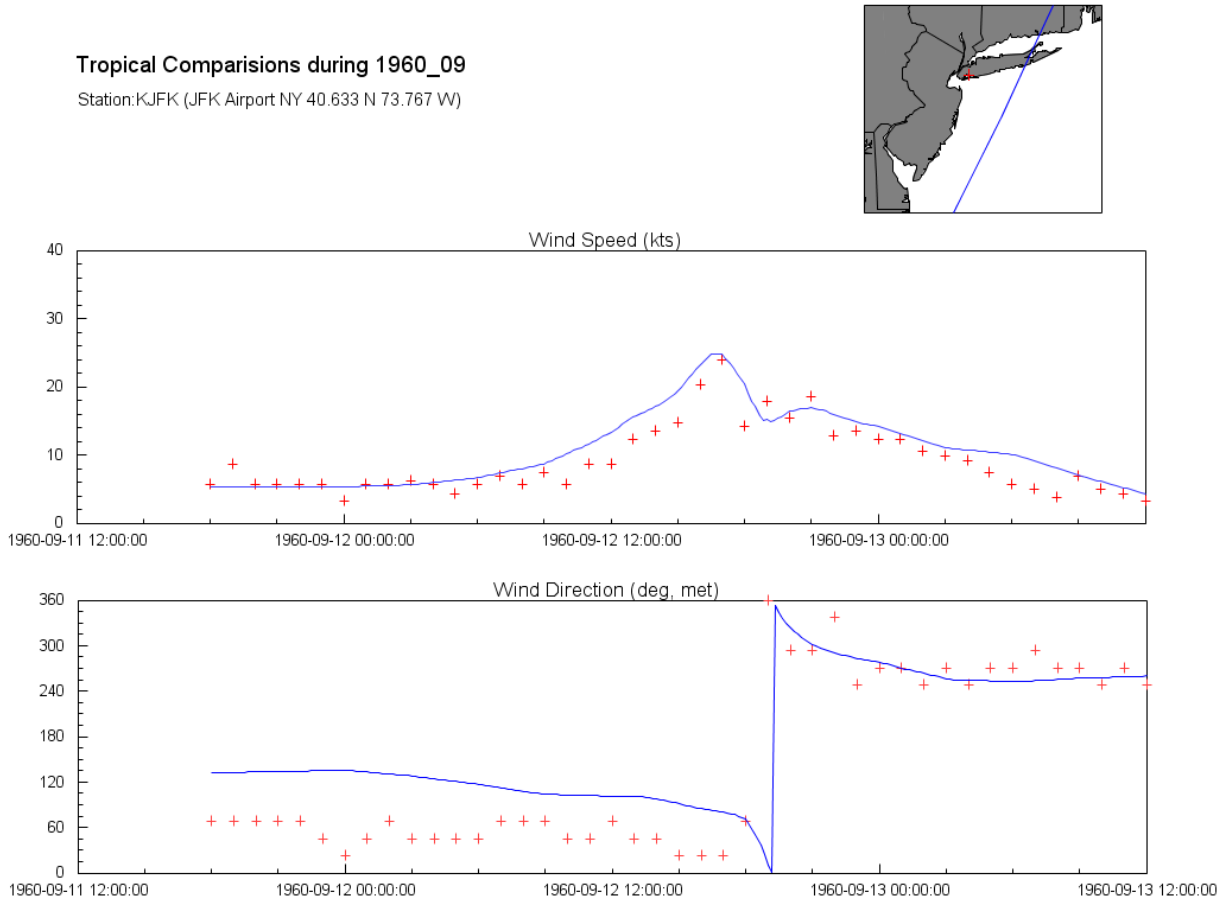

Figure 23. Wind speed and direction comparison at John F. Kennedy Airport during 1960_09.

4.2.4 Hurricane Gloria (1985)

Hurricane Gloria of 1985 made landfall at 16:00 UTC on September 27, 1985, with a central pressure of 957 mb and maximum 1-minute wind speeds of 70–75 knots. The radius of maximum winds at landfall was 30–35 Nmi. Tides were reported at the Battery, NY, as 7 feet above normal, according to NWS reports. Figure 24 depicts the storm track and envelope of maximum winds. The wind trace at Ambrose Light C-MAN station is shown in Figure 25.

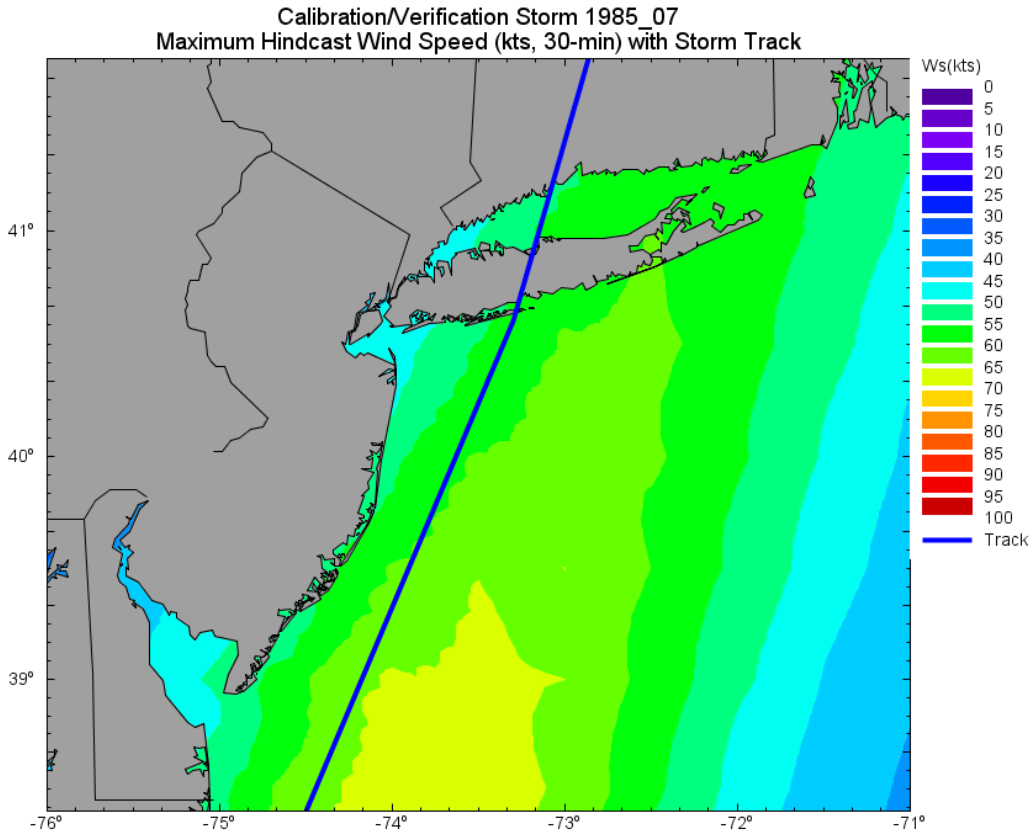

Figure 24. Maximum wind speed envelope (knots, 30-min) during 1985_07.

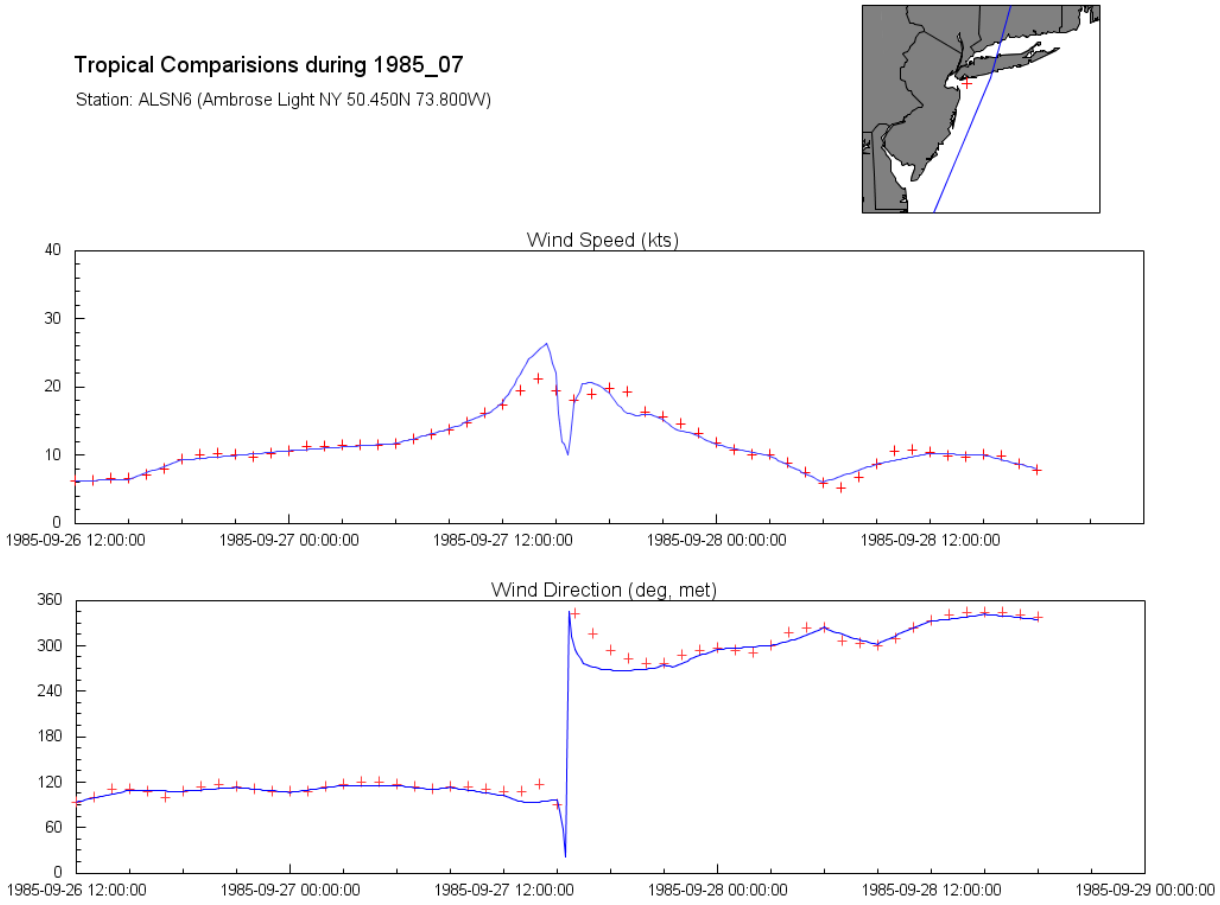

Figure 25. Wind speed and direction comparison at ALSN6 (Ambrose Light 50.45N 73.80W) during 1985_07.

4.3 EXTRATROPICAL STORM ANALYSIS

The 30 extratropical storms identified for hindcast are shown in Table 6 and include approximately a 5-day spin-up and 3-day spin-down period from the storm's peak surge. Storms were hindcast using the Interactive Objective Kinematic Analysis system as described in Cox et al., 1995. Wind and pressure data were obtained from the following sources:

1. National Centers for Environmental Prediction/National Center for Atmospheric Research (NCEP/NCAR) reanalysis wind and pressure fields
2. Buoy and C-MAN Coastal Manned Station data from National Data Buoy Center (NDBC)
3. National Weather Service (NWS) and National Ocean Service (NOS) land station data provided by the National Climatic Data Center (NCDC)
4. Ship reports from Comprehensive Ocean-Atmosphere Dataset (COADS)
5. Scatterometer wind estimates from the QUIKSCAT, ERS-1, ERS-2 instruments

Wind fields from individual storms were reanalyzed using kinematic analysis, a man-intensive process where wind speeds (isotachs) and wind directions (streamlines) are hand-drawn to best represent the available observations while preserving the primary meteorological principles of storm development and continuity. Figure 26 shows an example of a kinematic analysis valid during the October 1991 event. Figures of all storm quality control plots may be found in Appendix D.

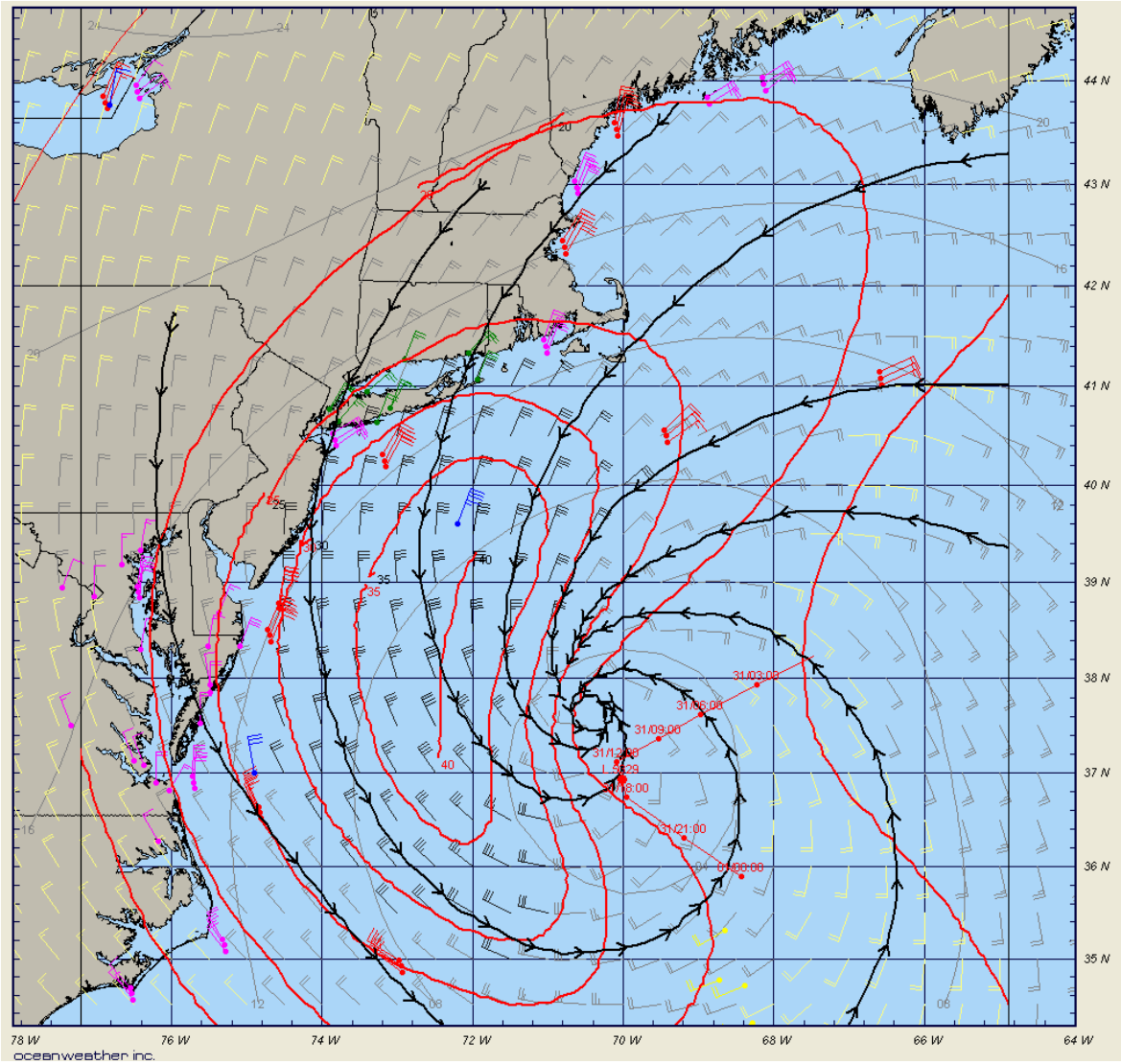

Figure 26. Example analysis of isotachs (red, knots) and streamlines (black) valid Oct-31-1991 15:00 UTC

SECTION FIVE PRODUCTION OF SYNTHETIC STORM WIND AND PRESSURE FIELDS

Production of synthetic storm wind and pressure fields was completed in two phases: JPM-Ref and JPM-OS1. JPM-Ref consisted of 4,108 storm events and was primarily used to drive a low resolution ADCIRC model to determine the final JPM set. JPM-OS1 storms were run through the fully coupled ADCIRC-UnSWAN modeling system. The JPM-OS1 set consisted of 159 storm events.

All the JPM source data were supplied by Lettis Associates and included the PBL model inputs specified every hour. Details on the JPM development are included in the separate Joint Probability Analysis report (RAMPP, 2014); however, a summary of each set is depicted in Figure 27. All storms begin on Jul-11-2000 01:00 UTC and end on Jul-16-2000 00:00 UTC regardless of translation speed. Landfall or time of closest approach is always indexed to Jul-15-2000 00:00 UTC in all input files. Initialization of PBL inputs is kept the same as in the calibration/verification phase, including capping the speed of the system at 25 knots in the dynamic wind solution. This cap relates only to the calculation of wind speed in the snapshot solution and does not constrain the storm's translation, which is preserved from the JPM track data. This cap is a standard procedure in applying the PBL model to prevent undue deformation of the wind solution at high storm translation speeds.

Wind speed and pressure outputs were generated on the two working grids at 15-minute intervals, as described in Section 4.1. Quality control plots included those shown in Figures 28 and 29. Figure 28 depicts the primary PBL inputs (pressure, scale pressure radius, track, and B) along with the resultant maximum wind speed and radius of maximum winds for the entire lifetime of the synthetic storm. Figure 29 depicts the surface 10-m wind field (30-minute average) and sea level pressure field at the time of landfall/closest approach. Figures of all storm quality control plots may be found in Appendix E.

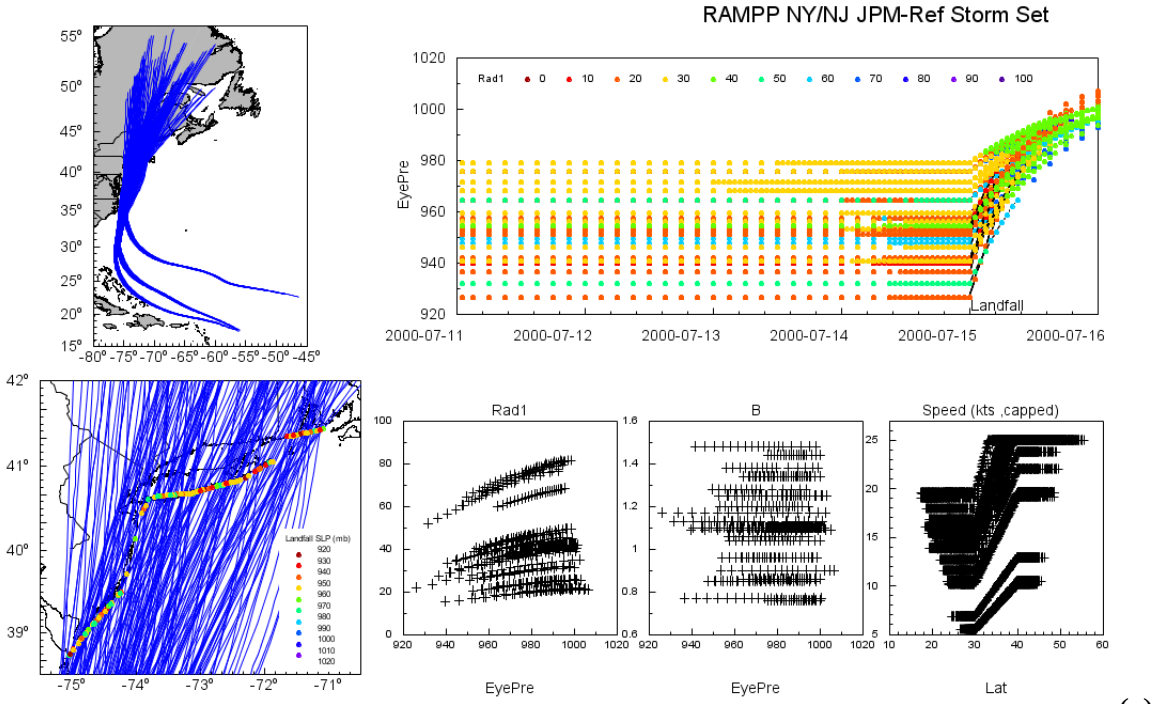

(a)

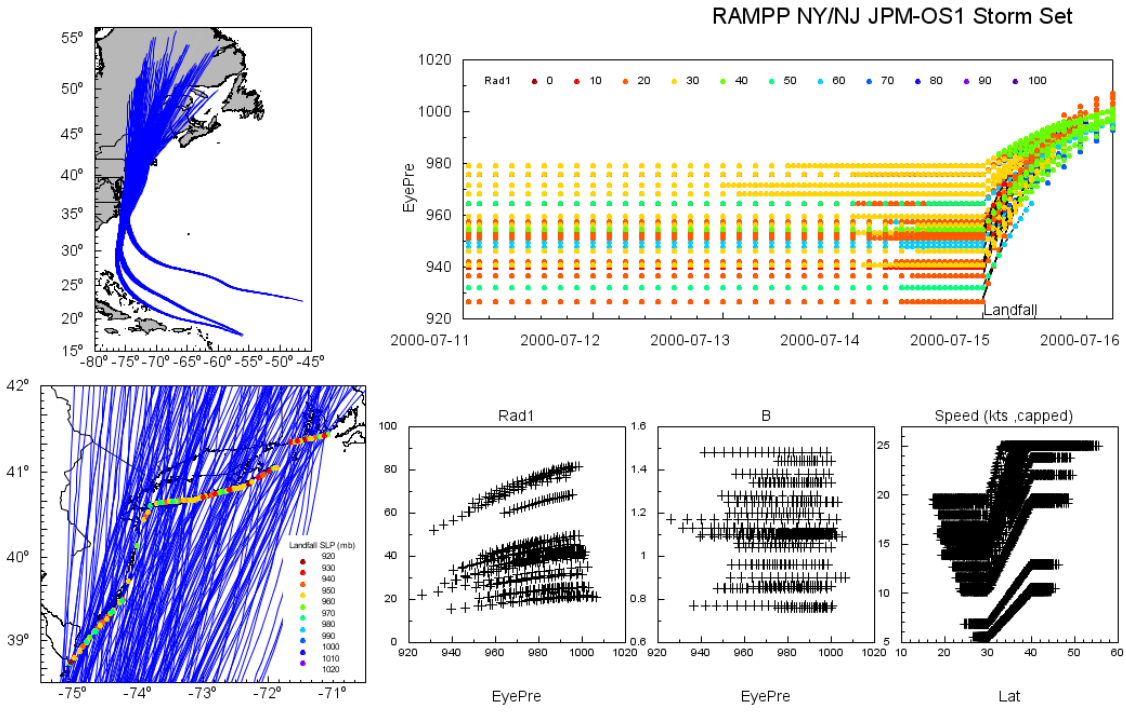

(b)

Figure 27. Summary of JPM-Ref (a) and JPM-OS1 (b) storm track and parameters

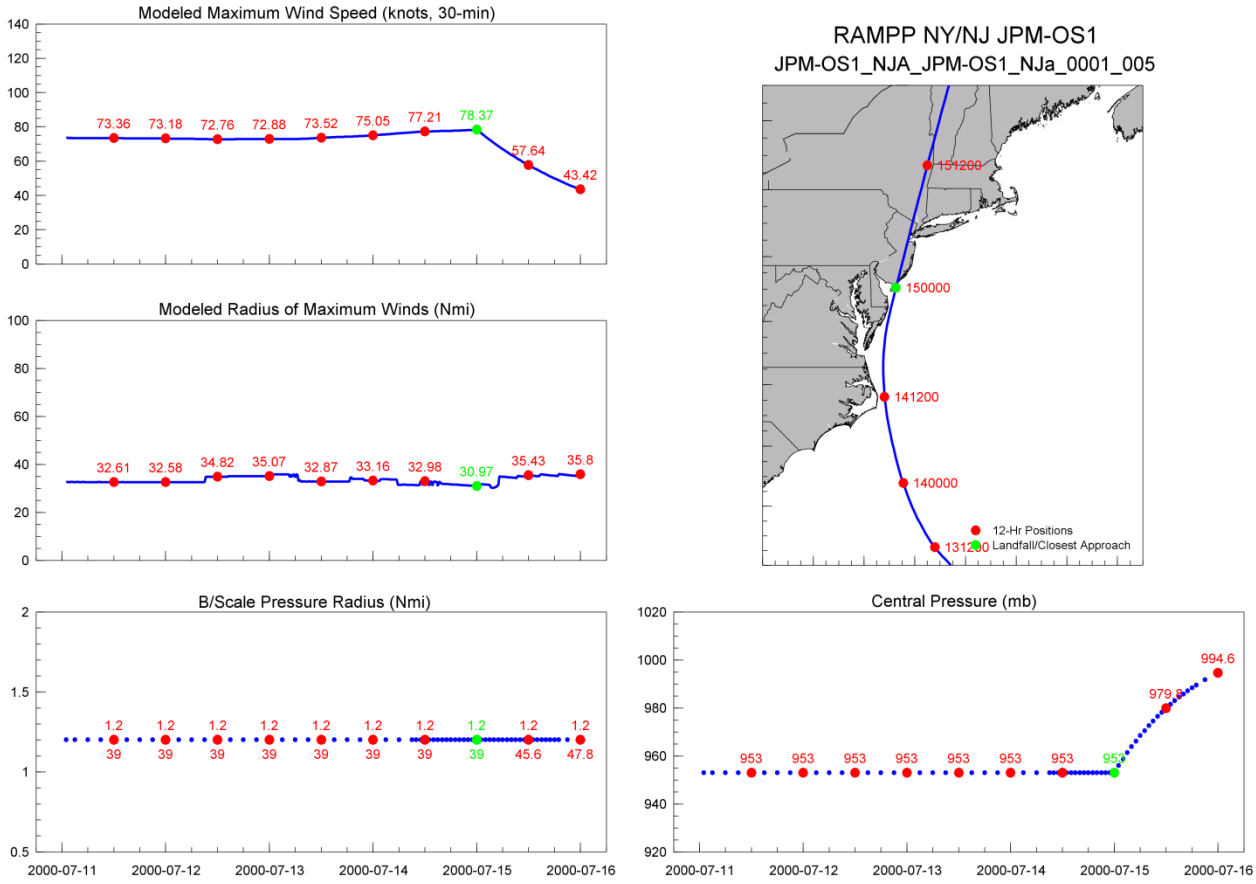

Figure 28. Summary of model inputs and wind output from the PBL model for JPM-OS1 track NJa_0001_005

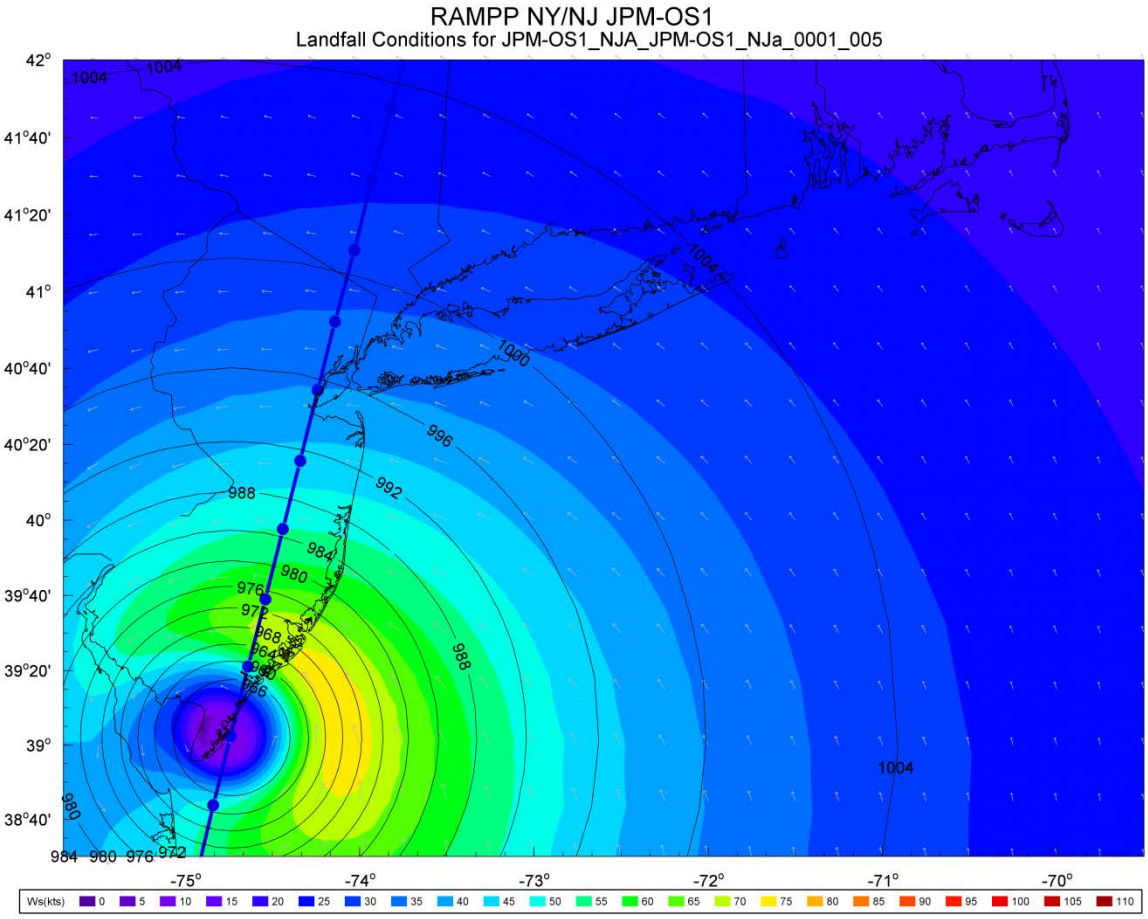

Figure 29. Wind speed (kts, 30-min) and pressures (mb) at landfall for JPM-OS1 track NJa_0001_005

SECTION SIX REFERENCES

Cardone, V.J. and C.K. Grant, Southeast Asia meteorological and oceanographic hindcast study (SEAMOS). OSEA 94132. 10th Offshore Southeast Asia Conference, 6–9 December, 1994.

Cardone, V.J. and D.B. Ross, State-of-the-art wave prediction methods and data requirements. Ocean Wave Climate ed. M. D. Earle and A. Malahoff. Plenum Publishing Corp., 1979, pp. 61–91.

Cardone, V.J., A.T. Cox, J.A. Greenwood, and E.F. Thompson, Upgrade of tropical cyclone surface wind field model. Misc. Paper CERC-94-14, U.S. Army Corps of Engineers, 1994.

Cardone, V.J., and A.T. Cox, Tropical cyclone wind field forcing for surge models: critical issues and sensitivities**.** Natural Hazards: Volume 51, Issue 1, 2009, p. 29.

Cardone, V.J., C.V. Greenwood and J.A. Greenwood, Unified program for the specification of tropical cyclone boundary layer winds over surfaces of specified roughness. Contract Rep. CERC 92-1, U.S. Army Engrs. Wtrwy. Experiment Station, Vicksburg, MS, 1992.

Cardone, V.J., J.G. Greenwood and M.A. Cane, On trends in historical marine wind data. J. Climate, 3, 1990, pp. 113–127.

Cardone, V.J., W.J. Pierson and E.G. Ward, Hindcasting the directional spectra of hurricane generated waves. J. of Petrol. Technol., 28, 1976, pp. 385–394.

Chow, S.H., A study of the wind field in the planetary boundary layer of a moving tropical cyclone. Master of Science Thesis in Meteorology, School of Engineering and Science, New York University, New York, NY, 1971.

Cox, A.T. and V.J. Cardone, Workstation assisted specification of tropical cyclone parameters from archived real time meteorological measurements. 10th International Workshop on Wave Hindcasting and Forecasting and Coastal Hazard Symposium. North Shore Oahu, 11–16 November, 2007. Available from Environment Canada, Downsview, ON.

Cox, A.T. and V.J. Cardone. Operational System for the Prediction of Tropical Cyclone Generated Winds and Waves. 6th International Workshop on Wave Hindcasting and Forecasting. November 6–10, 2000. Monterey, CA.

Cox, A.T., J.A. Greenwood, V.J. Cardone and V.R. Swail, An interactive objective kinematic analysis system. Proc. 5th International Workshop on Wave Hindcasting and Forecasting, Banff, Alberta, 16–20 October, 1995, pp. 109–118.

Forristall, G.Z., A two-layer model for hurricane driven currents on an irregular grid. J. Phys. Oceanog., 10, 9, 1980, pp.1,417–1,438.

Forristall, G.Z., E.G. Ward, V.J. Cardone, and L.E. Borgman, The directional spectra and kinematics of surface waves in Tropical Storm Delia. J. of Phys. Oceanog., 8, 1978, pp. 888–909.

Forristall, G.Z., R.C. Hamilton and V.J. Cardone, Continental shelf currents in tropical storm Delia: observations and theory. J. of Phys. Oceanog. 7, 1977, pp. 532–546.

Holland, G.J., An analytical model of the wind and pressure profiles in hurricanes. Mon. Wea. Rev. 1980, 108, pp. 1,212–1,218.

Kalnay, E., et al, *The NCEP/NCAR 40-Year reanalysis project*. Bull. Amer. Meteor. Soc., **77**, 3, 1996, pp. 437–471.

Knaff, J.A. and R.M. Zehr, Reexamination of Tropical Cyclone Wind-Pressure Relationships. Wea. and Fore., Volume 22, Feb 2007, pp. 71–88.

Landsea and Coauthors, The Atlantic hurricane database re-analysis project: Documentation for the 1851-1910 alterations and additions to the HURDAT database. 2004.

Landsea, C., M. Dickinson, and D. Strahan, Reanalysis of Ten U.S. Landfalling Hurricanes. Final report submitted to the Risk Prediction Initiative, 2008, 120 pp.

MORPHOS Report: Oceanweather Tropical Planetary Boundary Layer Model, 2009.

Pore, N.A. and C.S. Barrientos, Storm Surge. MESA New York Bight Atlas 6, New York Sea Grant Institute, 1976.

Powell, M.D. 2007. New Findings on hurricane intensity, wind field extent and surface drag coefficient behavior. 10th Workshop on Wave Hindcasting and Forecasting, Oahu, HI, Nov. 11-16, 2007.

Powell, M.D., D. Bowman, D. Gilhousen, S. Murillo, N. Carrasco and R. St. Fleur. Tropical Cyclone Winds at Landfall. Bull. Of AMS, June 2004 pp. 845–851.

Powell, M.D., S.H. Houston, L.R. Amat, and N. Morriseau-Leroy, The HRD Real Time Hurricane Wind Analysis System. J. Wind Engineer. and Indust. Aerodyn. 77&78, 1998, pp. 53–64.

RAMPP, 2014. Region II Storm Surge Project - Joint Probability Analysis of Hurricane and Extratropical Flood Hazards, FEMA TO HSFE02-09-J-001, 2014.

Ross, D.B. and V.J. Cardone, A comparison of parametric and spectral hurricane wave prediction products. Turbulent Fluxes through the Sea Surface, Wave Dynamics, and Prediction, A. Favre and K. Hasselmann, editors, 1978, pp. 647–665.

Shapiro, L.J., The asymmetric boundary layer flow under a translating hurricane. J. of Atm. Sci. 39, February 1983.

Thompson, E.F. and V.J. Cardone, Practical modeling of hurricane surface wind fields. ASCE J. of Waterway, Port, Coastal and Ocean Engineering. 122, 4, 1996, pp. 195–205.

Uhlhorn, E.W., P.G. Black, J.L. Franklin, M. Goodberlet, J. Carswell and A.S. Goldstein Hurricane Surface Wind Measurements from an Operational Stepped Frequency Microwave Radiometer, Mon. Wea. Rev. Volume 135, Sept. 2007, pp. 3,070–3,085.

Vickery, P.J. and P.F. Skerlj, Hurricane Gust Factors Revisited. Jour. Struct. Eng., Volume 131, No.5, May 2005.

Willoughby, H.E., R.W.R. Darling, and M. E. Rahn, Parametric representation of the primary hurricane vortex. Part II: a new family of sectionally continuous profiles. Mon. Weather. Rev.132, 2006, pp. 3,033–3,048.

Worley, S.J., S.D. Woodruff, R.W. Reynolds, S.J. Lubker, and N. Lott, ICOADS Release 2.1 data and products. Int. J. Climatol., 25, 2005, pp. 823–842.

Appendix A
Fits by Storm

Appendix B

Summary Plots of Model Parameters and Output

Appendix C
Tropical Characterization Database

Appendix D
Winter Storm Max Plots

Appendix E
JPM-OS1 Quality Control Plots